Long Title: Dynamic evolution of MLKL in primate and poxvirus genomes indicates necroptosis is a critical, not auxiliary, countermeasure during infection

Short Title: Dynamic evolution of host and viral necroptotic factors

Suzette Palmer[1], Sruthi Chappidi[1], Chelsea Pinkham[1] and Dustin C. Hancks[1*]

[1]Department of Immunology, University of Texas Southwestern Medical Center, Dallas, Texas, United States of America

* Corresponding author
E-mail: dustin.hancks@utsouthwestern.edu (DH)

Abstract

Pathogen infection triggers host innate defenses which can lead to the activation of regulated cell death (RCD) pathways such as apoptosis. Given a key role in immunity, apoptotic effectors are often counteracted by pathogen-encoded antagonists. Mounting evidence indicates that programmed necrosis, which is mediated by the RIPK3/MLKL axis and termed necroptosis, evolved as a countermeasure to pathogen-mediated inhibition of apoptotic signaling. However, whether this emerging inflammatory RCD pathway functions primarily as a “back-up” or fundamental response remains inconclusive. We hypothesized that if necroptosis is an instrumental defense, then its effectors should display specific signatures associated with pathogen conflict that are rare in combination: rapid evolution, viral homolog hereafter virolog, and induction by cytokines (e.g. interferons). Our rapid evolution analysis across the necroptosis pathway revealed: 1) strong signatures of positive selection for RIPK3 and MLKL in primate genomes and to a lesser extent DAI/ZBP1, 2) elevated rates of amino acid substitution on multiple surfaces including the RIPK3/MLKL binding interface and 3) evidence supporting a means of activating RIPK3 independent of homotypic RHIM domain interactions. Interestingly, a poxvirus MLKL homolog has recently been identified that acts as a RIPK3 pseudosubstrate. Our findings indicate that poxvirus MLKLs are also subject to similar but distinct volatile patterns of evolution comparable to host necroptotic factors. Specifically, viral MLKLs have undergone numerous gains and losses in poxvirus evolution with some species harboring three distinct copies. Furthermore, we confirm that MLKL can be induced by cytokines like interferon gamma. In summary, MLKL displays all three hallmarks of pivotal immune factors of which only OAS1, but not other factors

38 like cGAS, APOBEC3G, or PKR, exhibits. These data support the hypothesis that over
39 evolutionary time, necroptosis has served as a key battleground during infection and is
40 therefore, not an auxiliary response.
41

Summary

Regulated cell death (RCD), such as apoptosis, is a common host defense against invading pathogens. Necroptosis, an inflammatory RCD pathway, is thought to have emerged as an auxiliary response when other cell death pathways are suppressed by pathogens during infection. In our analyses, we have identified genetic changes in host and viral factors associated with necroptosis that display signatures of adaptation and may have served as evolutionary countermeasures to shape infection outcomes. Consistent with repeated targeting by pathogen-encoded inhibitors, we found robust signatures of rapid evolution for the essential catalysts of necroptosis, RIPK3 and MLKL. Notably, an evolutionary signature specific to RIPK3 for a domain shared with other necroptotic factors suggests an undefined means to trigger this host defense pathway. In contrast, poxviruses appear to circumvent this pathway by constantly altering the number and nature of factors they deploy to suppress necroptosis including a mimic of MLKL, which was stolen from infected cells. Collectively, our findings provide new insights into host and viral genetics that may influence infection outcomes and the factors shaping the ability of pathogens to infect and spread to new species. Furthermore, these data support the notion that necroptosis is a fundamental, not auxiliary, host response during infection.

Introduction

Regulated cell death (RCD) programs are pivotal host defense responses against pathogens [1-3]. Consequently, pathogens have evolved a myriad of strategies to counteract these responses [4, 5], which includes the activation of apoptosis. Apoptosis is a well-characterized, non-inflammatory form of RCD that was first classified by its distinct morphology that includes membrane blebbing, apoptotic bodies, and nuclear and cytoplasmic condensation [6]. Both extrinsic as well as intrinsic cues can trigger a signaling cascade that involves the activation of effector caspases to execute apoptosis (Fig 1A) [7] which was characterized, in large part, using viral proteins [8].

Recently, a RCD pathway defined as programmed necrosis, hereafter necroptosis, was discovered. Necroptosis is triggered when specific apoptotic signaling and effector functions are suppressed during pathogen infection. Given the conditions under which it is activated, necroptosis has often been considered a necessary “back-up” host response to pathogen-mediated inhibition of apoptosis (Fig 1B) [9, 10]. In contrast to apoptotic cell death, necroptosis is inflammatory and characterized by cell and organelle swelling followed by plasma membrane rupture [7, 11, 12]. Apoptotic and necroptotic signaling also differ in their evolutionary dynamics over large timescales. Specifically, key effectors of cellular necroptotic signaling emerged later in evolution and display a “patchy” phylogenetic distribution [13, 14] which is in marked contrast to the more ancient and highly conserved components of apoptotic signaling [15-17]. Notably, the evolutionary dynamics of necroptotic signaling over more recent timescales is unknown but may inform determinants shaping contemporary infections.

84 Necroptosis can be initiated by at least three presumably independent receptors:
85 1) death receptor (DR) signaling, 2) the pathogen recognition receptor (PRR) Z-DNA
86 Binding Protein 1 (ZBP1) / DNA Activator of Interferon (DAI), and 3) Toll-like Receptor 3/4
87 (TLR3/TLR4) [7]. Activation of DR signaling triggers Receptor Interacting Protein Kinase
88 1 (RIPK1) to self-oligomerize, which leads to the recruitment of Receptor Interacting
89 Protein Kinase 3 (RIPK3) via physical RIP Homotypic Interaction Motif (RHIM) domain
90 interactions. Activated RIPK3 subsequently binds and phosphorylates Mixed Lineage
91 Kinase-Like (MLKL) [18-20]. Phosphorylation of MLKL results in a conformational change,
92 enabling self-oligomerization of this factor to complete necroptosis through MLKL-plasma
93 membrane destabilization [21, 22].
94 Importantly, DR initiation of necroptosis appears to function when caspase-8
95 activity is inhibited during apoptosis [23, 24]. In contrast, DAI triggers necroptosis upon
96 binding foreign nucleic acids followed by activation of RIPK3 via RHIM-dependent
97 interactions [25, 26]. In addition, TLR3 and TLR4 signaling can activate RIPK3 via TIR-
98 domain-containing adaptor-inducing interferon-β (TRIF) also through physical RHIM
99 domain interactions [27, 28]. The diverse and distinct means of activating necroptosis with
100 convergence on the RIPK3/MLKL axis reflect the breadth of pathogens this response may
101 protect against.
102 Consistently, a growing list of viral- and bacterial-encoded inhibitors that target
103 discrete steps of necroptosis has emerged [29-36]. However, whether this pathogen-
104 mediated antagonism has shaped cellular necroptotic factors remains unknown. Strong
105 selective pressure may be imposed on host factors to escape direct binding by pathogen-
106 encoded antagonists. This pressure is often visible as elevated rates of amino acid

107 substitution, a signature of rapid evolution and a hallmark of positive selection. Signatures
108 of rapid evolution have been observed across orthologous sequences from closely related
109 species (e.g. primates) for several key immune factors: PKR [37], OAS1 [38, 39], MxA [40],
110 TRIM5α [41], APOBEC3G [41], and cGAS [38, 39]. Studies of host-pathogen co-evolution
111 may reveal novel insights into cellular responses including evidence for undefined host
112 components, genetic determinants shaping infection outcomes, and pathogen
113 countermeasures of these defenses. We hypothesized that analysis of signatures
114 characteristic of host-pathogen conflict for both cellular and viral components would
115 illuminate whether necroptosis has served as a "back-up" or a core, fundamental
116 response over evolutionary time.

117 Consistent with pivotal roles in host defense across species, we report that the
118 necroptotic axis in primates - RIPK3 and MLKL - displays widespread and recurrent
119 signatures of rapid evolution. Interestingly, we found evidence for positive selection within
120 the RHIM domain of RIPK3, but not at homologous sites in RHIM domains of DAI, TRIF,
121 or RIPK1, that is proximal to a known target-site for a conserved bacterial protease.
122 Notably, these bacterial proteases have been shown to cleave all of the RHIM domain
123 containing necroptosis factors [30]. These data suggest an undefined means of RHIM-
124 independent RIPK3 activation. Evolutionary genetics analysis of a recently described
125 poxvirus MLKL homolog indicate that this antagonist has been subjected to repeated
126 gains and losses over viral evolution with some poxvirus genomes encoding up to three
127 mimics. In summary, our data demonstrate that MLKL belongs to a small class of key
128 immune factors, which includes OAS1 but not PKR or cGAS, that display all three
129 hallmarks of pivotal immune factors - rare in combination: 1) rapidly evolving, 2) viral

homolog, and 3) upregulation by cytokines such as interferons. Collectively, our data are consistent with necroptosis being a fundamental host defense, not an auxiliary one, shaping infection outcomes over evolution.

Results

Widespread signatures of rapid evolution in primate RIPK3 and MLKL

To determine if known components of the necroptosis pathway display signatures of positive selection, we analyzed a matching set of twenty-one primate sequences for *TRIF*, *DAI*, *RIPK1*, *RIPK3* and *MLKL* using a series of evolutionary analyses. To test for recurrent positive selection, we used a combination of maximum-likelihood based algorithms, which estimate rates of non-synonymous amino acid replacements (dN) relative to synonymous (dS) amino acid substitutions. dN/dS values > 1 are considered a hallmark of positive selection. Using codon-based models implemented in Phylogenetic Analysis by Maximum Likelihood (PAML) [42], we detected robust gene-wide rapid evolution signatures for *MLKL* [M7 vs. M8 (F3x4) $p < 5.400 \times 10^{-10}$], *RIPK3* [M7 vs. M8 (F3x4) $p < 3.056 \times 10^{-9}$] and to a lesser extent, *DAI* [M7 vs. M8 (F3x4) $p < 5.767 \times 10^{-3}$] but not *RIPK1* [M7 vs. M8 (F3x4) $p < 0.065$] or *TRIF* [M7 vs. M8 (F3x4) $p < 0.066$] (Fig 2A, S1 File). The signature of selection for the main effectors of the necroptosis pathway, RIPK3 and MLKL, is comparable to other key host defense factors – PKR, cGAS, OAS1 – which are also upregulated by cytokines. Indeed, MLKL is also upregulated by cytokines like interferons [43-45], which we confirm for IFNγ (Fig 2B).

To assay when and to what extent selection pressure has shaped necroptotic signaling over primate evolution, we estimated dN/dS values across the primate phylogeny (Fig 2C) for each factor. Consistent with our gene-wide tests of evolution, we

154 observed recurrent and widespread signatures of positive selection across primates for
155 *RIPK3*, *MLKL* and again to a lesser extent, *DAI*. Specifically, numerous lineages across
156 primate evolution for both *RIPK3* and *MLKL*, including branches in each major group,
157 show substitution patterns that are characteristic of genetic conflict. Strikingly, especially
158 strong signatures are evident for *RIPK3* in the lineage preceding the divergence of
159 Hominidae [10 nonsynonymous changes: 0 synonymous changes] and for *MLKL* in the
160 lineage prior to Hominidae divergence [dN/dS = 4.49] (Fig 2C). In contrast, only one
161 lineage with a rapid evolution signature was detected for both *TRIF* and *RIPK1*. Thus,
162 repeated innovation in the necroptosis pathway has been primarily focused on the
163 downstream axis of *RIPK3*/*MLKL* during primate evolution.

164 To uncover where strong selection pressure may have been imposed within the
165 effector proteins of necroptosis, dN/dS values were estimated for individual amino acid
166 positions using three distinct but commonly implemented methods: PAML [42], MEME
167 [46], and FUBAR [47] (Fig 3A, S1 File). The distribution and the number of rapidly evolving
168 sites are thought to reflect the number of protein surfaces in genetic conflict with other
169 factors, such as pathogen-encoded inhibitors [48]. In agreement with necroptosis being
170 triggered by diverse pathogens, predicted rapidly evolving sites are distributed throughout
171 the necroptosis proteins (*MLKL*, *RIPK3*, *DAI*, *RIPK1*, and *TRIF*). In support of our
172 preceding analysis, *MLKL* (20 total sites / 11 by multiple methods) and *RIPK3* (27 total
173 sites / 7 by multiple methods) have the most sites identified (Fig 3A). Interestingly, the
174 majority (70%) of MLKL positively selected sites are localized to the kinase-like domain,
175 with 12/14 sites within this domain occurring between amino acid positions 370-470 (Fig
176 3A). Positively selected sites mapped onto a previously published co-crystal structure of

177 mouse RIPK3 and MLKL [49] indicate that clusters of sites represent distinct surfaces (Fig
178 3B). Analysis of space-filling models highlights that the majority of the rapidly evolving
179 sites are found on the protein surface for both RIPK3 and MLKL, which suggests they
180 represent interfaces for protein-protein interactions (S1 Fig). Notably, there is a cluster of
181 positively selected sites for RIPK3 that surrounds MLKL and corresponds to the
182 hydrophobic pocket where RIPK3 and MLKL interact via hydrophobic interactions (Fig
183 3C). This signature may indicate the presence of MLKL pseudosubstrates, as this pocket
184 has been demonstrated previously to be necessary for RIPK3:MLKL interaction and for
185 necroptosis to occur [31, 49].

186 **Rapid evolution exclusive to the RHIM domain of RIPK3 localizes to a known**
187 **bacterial protease cleavage site**
188
189 RHIM-RHIM homotypic interactions between RIPK3 and established necroptosis
190 activators RIPK1, TRIF, and DAI are required for signal transduction. The critical nature
191 of this interaction is also supported by the identification of both viral- and bacterial-
192 encoded inhibitors that target the RHIM domains of these proteins. These include
193 cytomegalovirus M45 and herpes simplex virus ICP6 and ICP10, which all encode RHIM
194 domains and target host RHIM-dependent interactions [29, 33]. Another example is EspL,
195 a bacterial protease, which is encoded by diverse species, including enteropathogenic
196 *Escherichia coli* (EPEC), *Salmonella enterica,* and *Yersinia pestis* [30]. Notably, EPEC
197 EspL has been shown to cleave a specific motif (Q*G**N) in the RHIM domains of human
198 and mouse TRIF, DAI, RIPK3, and RIPK1, which results in the suppression of necroptosis
199 [30]. Interestingly, rapid evolution was evident in the RIPK3 RHIM domain but not
200 detectable in homologous domains across primate *TRIF*, *DAI,* and *RIPK1* (Fig 3D).
201 Indeed, *RIPK3* showed elevated rates of substitution by PAML analysis at two sites

202 immediately adjacent to the determined RHIM EspL cleavage motif – GDN/NYL where "/"
203 indicates cleavage; the sites 462D and 463N are rapidly evolving (Fig 3D). The
204 evolutionary signatures of necroptosis RHIM domains may indicate modes of RIPK3
205 activation and/or functions independent of the RIPK1, TRIF, and DAI RHIM domains.

206 **Poxviral antagonism of the RIPK3:MLKL interface serves as a model for**
207 **antagonistic coevolution**
208
209 The rapid evolution signature of RIPK3 near the hydrophobic pocket indicates
210 antagonism, likely by pseudosubstrates (Fig 3C). Indeed, a viral copy of MLKL (vMLKL),
211 which is encoded by numerous poxviruses has been recently identified [31]. Yet, the
212 origins and evolution of these vMLKLs remain unknown. We identified twenty-seven
213 distinct copies of vMLKL in the sequence database across the genomes of *Avipoxvirus*,
214 Clade II, along with two other poxvirus species that infect bats [eptesipoxvirus (EPTV)
215 and hypsugopoxvirus (HYPV)] (Fig 4D). vMLKL lacks the N-terminal bundle and brace
216 (NBB) domain but maintains the C-terminal kinase-like domain, to which RIPK3 binds to
217 phosphorylate the host cellular homolog [31] (Fig 4A). Ectopic expression of two vMLKLs
218 from poxvirus species that primarily infect mice were demonstrated to competitively inhibit
219 both mouse and human RIPK3 in binding and cell-culture necroptosis assays [31].
220 Superposition of a homology model of myxoma virus (MYXV) MLKL onto published
221 crystal structures for mouse MLKL [49] and human MLKL [50] indicated striking structural
222 overlap with human and mouse MLKL (Fig 4B). This occurs despite a broad-range of
223 amino acid divergence between these host and viral MLKLs (16-25% amino acid identity
224 of the virus homologs to mouse and human MLKLs).
225 In agreement with the strong structural overlap, characterization of vMLKL
226 sequences indicate conservation of functional residues for human and mouse MLKL

227 including ATP binding, hydrogen-bonding, and protein stability (S2A Fig) [19-21, 49-51].
228 Several amino acid sites displaying positive selection for MLKL (Figs 2 and 3) overlapped
229 or were in close proximity to sites for hydrogen bonding and protein stability, as
230 demonstrated by the amino acid alignment (S2A Fig). Of note, there are several intriguing
231 examples of specific residue conservation between the primate positively selected sites
232 and the viral copies. One example is human MLKL F386 (F373 mouse), which has been
233 shown to be necessary for RIPK3/MLKL complex formation [31]. This position exclusively
234 has tyrosine, phenylalanine, or histidine amino acid variants across the sampled primates,
235 with this pattern of aromatic residues evident and conserved to Aves MLKL virologs (S2B
236 Fig). Consistently, poxvirus virologs have also maintained only aromatic (phenylalanine
237 or tyrosine) amino acids at the homologous position (S2A Fig). These data suggest a key
238 role for site 386 in host defense but also in counteraction by viral mimics [52].

239 To further understand the evolutionary relationships between poxvirus vMLKLs,
240 we performed detailed sequence and phylogenetic analyses across corresponding viral
241 genomes. Full-length vMLKLs (excluding partial Vulture gryphus poxvirus and Hawaiian
242 goosepox virus sequences) display 18%-100% amino acid identity relative to each other
243 and cluster in a manner resembling known poxviral species relationships (Fig 4C).
244 Unexpectedly, this analysis identified two distinct vMLKL copies (e.g. paralogs), which
245 differ in amino acid identity, in the genomes of both eptesipoxvirus (EPTV vMLKL-A vs.
246 EPTV vMLKL-B : 45% amino acid identity) and hypsugopoxvirus (HYPV vMLKL-A vs.
247 HYPV vMLKL-B : 43% amino acid identity). Analysis of the location of the different
248 vMLKLs in each genome was conducted using CoGeBlast, which allows for individual hit
249 visualization. The results suggested distinct genomic locations for these genes (Fig 4E).

250 Specifically, a majority of vMLKLs are located primarily on the right arm of the poxvirus
251 genome with EPTV having two copies that map to two distinct loci in this region. In
252 addition, both HYPV and EPTV have one additional copy that maps to the left arm of the
253 poxvirus genome. Interestingly, two of the vMLKLs in EPTV are present on the inverted
254 terminal repeat (ITR), potentially representing more recent acquisitions. Likewise, fowlpox
255 virus-282E4 vMLKL appears to be at a distinct inverted locus relative to other *Avipoxvirus*
256 species on the left arm of the genome (Fig 4E).

257 To confirm additional vMLKL copy numbers present in the eptesipoxvirus genome,
258 we next performed relative depth analysis, with approximately 1000 - fold genome
259 coverage (Fig 4F, S3 Fig), using the raw reads from the genome sequencing. By mapping
260 reads across the unique genome and one reference ITR, we found that EPTV – A/C has
261 a relative depth of two and EPTV – B has a relative depth of one, which supports the
262 presence of three copies in the eptesipoxvirus genome (Fig 4F). As a control, we also
263 conducted a similar analysis using reads from a recent myxoma virus sequencing project
264 [53] and found that the vMLKL relative depth remained near one, indicating the presence
265 of only one genomic copy (S3 Fig). These data demonstrate that vMLKLs have different
266 evolutionary histories and are likely not orthologous.

267 **Phylogenetic distribution of vMLKLs can account for variable conservation of E3**
268 **across species**
269
270 Poxviruses encode numerous immunomodulators to subdue and circumvent host
271 defenses including apoptosis. As a majority of poxviruses encode several characterized
272 anti-apoptotic proteins [54, 55] (Fig 4G, S4 Fig, S2 File) including the serpin class of
273 caspase pseudosubstrates [56, 57], these viruses would be expected to trigger
274 necroptosis. Indeed, the model poxvirus vaccinia has been shown recently to trigger

275 necroptosis through activation of DAI/ZBP1 in cultured cells and to counteract this
276 response using the Z - nucleic acid binding (Zα) domain of the E3 protein [32]. E3 is
277 considered a key host-range gene that antagonizes several host defenses. Interestingly,
278 some poxviruses that encode a repertoire of anti-apoptotic proteins lack E3 or possess
279 truncated E3 ORFs. For example, the *Avipoxvirus* family does not possess any orthologs
280 of E3 (Fig 4G, S2 File) and several Clade II poxviruses, including the well-characterized
281 myxoma virus, are also predicted to have N-terminally truncated E3 copies which lack the
282 Zα domain that is important for antagonism of DAI [55] (Fig 4G, S2 File). To gain insights
283 into how a subset of poxviruses may circumvent necroptosis given the presumed ability
284 to trigger apoptosis, we compared the breadth of known anti-apoptotic proteins, including
285 serpins, across the poxvirus phylogeny relative to vMLKL (Fig 4G). As vMLKLs are
286 present in *Avipoxvirus*, hypsugopoxvirus, myxoma virus and rabbit fibroma virus – the
287 maintenance of this pseudosubstrate may account for the tolerance of these species to a
288 missing or truncated E3 protein.

289 **Repeated gains and losses of vMLKL over poxvirus evolution**

290 Our data illustrates that multiple vMLKL copies may exist in a given poxvirus
291 genome and that not all of the copies across the genomes may be orthologous. To
292 determine the relationship of poxvirus vMLKLs, we performed a synteny analysis using
293 five flanking upstream and downstream genes across the entire phylogeny (Fig 5, S3
294 File). These data indicate that while each vMLKL within *Avipoxvirus* and Clade II are
295 flanked largely by the same upstream and downstream genes, vMLKLs between the
296 species are flanked by different genes. The Clade II and *Avipoxvirus* species have distinct
297 copies as indicated by different upstream and downstream genes. Furthermore, the lack

298 of vMLKL in Yatapoxvirus species (Yaba monkey tumor virus and Yaba-like disease
299 virus), which belong to Clade II, revealed that this loss is likely due to a deletion event
300 consisting of multiple upstream and downstream genes in these lineages (Fig 5, S3 File).
301 This analysis also provided insights regarding the multiple vMLKL copies in
302 eptesipoxvirus and hypsugopoxvirus. First, this analysis indicated that EPTV-B (EPTV-
303 WA-166) and HYPV-B (QDJ95132.1) are orthologous to each other and are likely
304 orthologous to the Clade II copies, as evidenced by some overlap in syntenic gene
305 neighbors (Fig 5). Second, EPTV-A (EPTV-WA-006) and HYPV-A (QDJ94987.1) share
306 gene neighbors indicating that these sequences are likely orthologs. EPTV-A shares
307 100% identity with EPTV-C (EPTV-WA-186) with both annotated as being located in the
308 inverted terminal repeats (ITRs). Consistently, EPTV-C has the same gene neighbors as
309 EPTV-A albeit inverted. The copies are labeled corresponding to their location starting
310 from the left arm of the poxvirus genome – e.g., A, B, C.
311 To further assess the evolutionary relatedness of vMLKLs, we performed whole
312 genome comparisons using CoreGenes (https://coregenes.ngrok.io/). This data was
313 visualized with RIdeogram [58] and focused on the copies encoded by *Avipoxvirus*, Clade
314 II and the two poxvirus species that primarily infect bats. Indeed, we found that canarypox
315 virus vMLKL and myxoma virus vMLKL localize to distinct chromosomal locations with no
316 shared surrounding regions of synteny (S5A Fig). In agreement with our local synteny
317 analysis above, the locus encoding Clade II vMLKL was likely lost in a Yatapoxvirus
318 ancestor following divergence as evidenced by global as well as local synteny
319 surrounding the vMLKL locus (S5B Fig). Lastly, we compared eptesipoxvirus with
320 myxoma virus (S5C Fig). The upstream regions of synteny of vMLKL indicate that MYXV

321 vMLKL is orthologous to the EPTV-B vMLKL copy, which is further supported by MYXV
322 vMLKL not being in the ITRs corresponding to EPTV-A/C. These data suggest vMLKLs
323 are at distinct loci in poxvirus genomes as a result of repeated gains and losses during
324 poxvirus genome evolution.

325 **Phylogenetic analysis reveals origination of vMLKL copy from one horizontal gene**
326 **transfer event**
327
328 The distinct copies of vMLKLs may have originated due to either 1) a single transfer
329 event from a host genome to an ancestral poxvirus followed by diversification or 2)
330 multiple independent transfer events from presumably distinct host genomes to different
331 poxviruses. To address this, we performed a phylogenetic analysis using amino acid
332 sequences of vMLKLs with thirty-eight diverse host MLKLs. If distinct vMLKLs were
333 acquired via independent events, placement of viral sequences would vary across the
334 tree in a manner where they pair with different host sequences. Such topology could
335 reflect the source genome or that of a related, perhaps ancestral, animal host. In contrast,
336 if vMLKLs originated from a single transfer event, the tree topology would group these
337 sequences into one clade. Phylogenetic analysis using PhyML [59] revealed that vMLKL
338 virologs cluster as one group distinct from animal vMLKLs (Fig 6). These data support a
339 single transfer event from an ancestral host genome as the most parsimonious origin for
340 vMLKL (Fig 6, S4 File). The topology of the poxvirus branches mirrors that of known
341 species relationships. For example, all of the *Avipoxvirus* species cluster together.
342 Likewise, the Clade II species cluster together broadly, as well as at a finer level such as
343 in the *Leporipoxviruses* (e.g. MYXV and RFV). The tree topology also supports the
344 synteny analysis with HYPV-B and EPTV-B being most closely related along with EPTV-
345 A/C and HYPV-A vMLKL clustering distinctly.

346 Still, it remains unclear whether Clade II vMLKLs represent a distinct or
347 orthologous locus to Avipox vMLKL and which vMLKL locus represents the ancestral
348 locus. Indeed, our data for Clade II vMLKL could be explained, in part, by either 1) a
349 duplication of the Avipox vMLKL locus followed by a deletion event of the original locus
350 in the Clade II ancestor or 2) that Avipox and Clade II vMLKL are orthologous but
351 divergence no longer allows for syntenic comparison between these species. We
352 assessed the likelihood of these evolutionary histories by analyzing patterns of amino
353 acid variation shared between vMLKLs and mammalian MLKLs, which cluster closest to
354 vMLKLs (Fig 6). We evaluated innovations specific to vMLKLs but not host MLKLs across
355 our alignment. We identified seventeen amino acid residues largely conserved between
356 Avipox vMLKLs and mammalian MLKLs (Fig 7) but not Clade II, EPTV and HYPV
357 vMLKLs. Conversely, different variants at the same sites are shared across Clade II,
358 EPTV and HYPV vMLKLs but not Avipox or mammalian MLKLs. These data support the
359 hypothesis that Avipox vMLKL is the original locus and that Clade II vMLKL is a distinct
360 copy but derived from the Avipox vMLKL presumably through duplication. Collectively,
361 these data illustrate a volatile history of vMLKL since its acquisition by an ancestral
362 *Avipoxvirus*.

363 **Discussion**

364

365 Studies of host-pathogen co-evolution can reveal new insights that forge infection
366 outcomes. These include vulnerabilities in host defense and determinants that shape
367 pathogen host range as well as zoonoses. In addition, analysis of host and pathogen
368 effectors can illuminate new evolutionary paradigms such as the evolutionary trajectories
369 of viral mimics. Here, we focused on the emerging regulated cell death program of

370 necroptosis that is largely presumed to be a “back-up” response. Our data, particularly
371 the robust signatures of positive selection in RIPK3/MLKL, mirrors that of key immune
372 factors like cGAS, PKR, and OAS1 [37, 38]. These features support the essentiality of
373 RIPK3/MLKL in immunity during primate evolution. In addition, the maintenance, as well
374 as gains and losses of vMLKL throughout poxvirus evolution, showcases the need to
375 actively counteract the necroptosis program.

376 **Proposed model for vMLKL acquisition**
377
378 The findings from our evolutionary analysis for vMLKL are consistent with a model
379 consisting of a series of gains and losses of this virolog over time (Fig 8A). Our data
380 paired with those of Petrie *et al*., which also suggested a host origin for vMLKL [31],
381 support the notion that this gene was initially acquired via one horizontal gene transfer
382 event (Fig 6). As vMLKL mirrors a truncated copy of cellular MLKL lacking introns, we
383 hypothesize that this transfer likely occurred via an RNA intermediate. The N-terminal
384 truncation in vMLKL could have transpired either during or after integration. This copy at
385 the original site of integration has been maintained through evolutionary time in
386 *Avipoxvirus* species and represents locus 1. Following the Avipox ancestral divergence
387 from a common ancestor shared with Clade II and HYPV/EPTV species, locus 1 appears
388 to have been duplicated to produce locus 2. We hypothesize that locus 1 was deleted
389 while locus 2 was maintained in the shared ancestor Clade II/EPTV/HYPV, and is present
390 today in most contemporary genomes of Clade II poxviruses and EPTV-B/HYPV-B. Yet,
391 it remains possible - due to extensive rearrangements resulting in the degradation of any
392 detectable synteny by either method we employed here - that locus 1 across Avipox
393 represents the Clade II/EPTV/HYPV vMLKL. In Yatapoxviruses, locus 2 vMLKL was lost

394 in what appears to be a multi-gene deletion event (Fig 5, S5 Fig). Following divergence
395 of the EPTV/HYPV ancestor from Clade II poxviruses, locus 2 was duplicated to a region
396 in the ITR with a subsequent duplication occurring in the other ITR. Both vMLKL copies
397 in the eptesipox ITRs are supported by our relative depth analysis (Fig 4F, S3 Fig). A
398 similar analysis was attempted but not possible with the hypsugopox genome data. Thus,
399 vMLKL resides at four distinct loci in poxvirus genomes across the phylogeny.

400 **Positive selection signatures in the necroptotic signaling pathway are localized to**
401 **the RIPK3/MLKL axis**

402 The signatures of rapid evolution in RIPK3 and MLKL resemble "molecular arms
403 races" dynamics with pathogen-encoded inhibitors [48] (Fig 2). The broad distribution of
404 rapidly evolving sites in both RIPK3 and MLKL is indicative of multiple, undefined
405 antagonists that have existed over evolutionary time (Fig 3). Interestingly, our analysis
406 across the core circuitry of necroptosis enabled two key observations. First, strong
407 selective pressure has been primarily exerted on the downstream components of the
408 pathway where upstream signaling converges (Figs 2 and 3). Second, our evolutionary
409 analysis across the pathway allowed the identification of rampant positive selection
410 exclusive to the RHIM-domain of RIPK3 but not the RHIM-domains of the upstream
411 activators DAI, TRIF, or RIPK1 (Fig 3). This is extremely striking given the elevated dN/dS
412 ratios for RIPK3, but not the other factors, at amino acid positions that define a
413 demonstrated cleavage site (Fig 3D) for the conserved bacterial protease EspL which is
414 capable of cleaving RHIM domains across this pathway. Notably, rapid evolution in the
415 adaptor protein MAVS has been shown to shape the ability of the hepatitis protease
416 NS3/4A to cleave this target [60]. Our data suggest that there may be RIPK3 activity that

417 is independent of activation by RHIM homotypic interactions (e.g., DAI/TRIF/RIPK1),
418 which is counteracted by EspL-like proteases. One possible explanation for this signature
419 is the presence of a yet undefined upstream activator of RIPK3, which lacks a RHIM-
420 domain, that is triggered by pathogenic bacteria. Given the data, we are unable to infer
421 whether this predicted activity of RIPK3 would also activate MLKL. Nevertheless, a
422 pathway perspective combined with evolutionary insights can drive new avenues of
423 investigation.

424 **RIPK3/MLKL as a model for the maintenance of compatible, functional interactions**

425 Our study describes volatile evolution of vMLKL in poxvirus genomes. This work
426 extends on the recent discovery of this mimic, which showed two vMLKLs are capable of
427 counteracting necroptosis in cell culture [31]. Our integrated comparison of established
428 poxvirus immunomodulators with the phylogenetic distribution of vMLKL appears to
429 resolve the long-standing conundrum of how some poxvirus species persist with N-
430 terminally truncated or completely absent E3 ORFs (Fig 4F). In addition, the lack of
431 vMLKLs in orthopoxviruses can be explained, in part, by the recent identification of vIRD
432 encoded by this genus, which is an ankyrin-repeat domain containing protein that targets
433 RIPK3 for degradation [35]. The resolution of the evolutionary history of vMLKL in our
434 study may serve as a resource in guiding the functional analysis of host and viral MLKL
435 variants and their impact on RIPK3 binding and activity. It has not escaped our attention
436 that the RIPK3/MLKL axis, in part, resembles another well-defined host defense axis -
437 PKR/eIF2 α - which also consists of a kinase and its substrate counteracted by a different
438 poxvirus pseudosubstrate (K3L) [37]. However, a major difference between the two
439 systems is that RIPK3 and MLKL are rapidly evolving, in contrast to PKR rapidly evolving

440 and eIF2α being ultraconserved to yeast. This is interesting given the PKR/eIF2α system

441 has been useful in understanding how a rapidly evolving factor maintains its interaction
442 with a conserved factor while evolving to escape antagonism [37]. Perhaps RIPK3/MLKL
443 may be powerful in understanding how two key host defense factors maintain their
444 essential interaction to drive necroptosis while escaping pathogen-mediated inhibition,
445 particularly pseudosubstrates similar to vMLKL.

446 **MLKL is a pivotal immune factor**

447 Our study defines MLKL, which functions as the executioner of necroptosis, as a
448 factor that 1) is (up)regulated by immune signals (Fig 2B) [43-45], 2) has a viral
449 homolog/virolog (Figs 4,5,6 and 7)[31] and 3) is rapidly evolving (Figs 2 and 3). While
450 several key host defense factors typically display two of these signatures, to our
451 knowledge, only a select few are published which display all three of these hallmarks (Fig
452 8B): OAS1 [38, 39, 61], and the recently described MISTRAV and MISTR1 [62]. OAS1 is
453 one of the first interferon-stimulated genes identified and functions in host defense against
454 numerous, diverse viruses [63]. MISTR proteins appear to interface with electron transport
455 chain complexes to regulate stress responses and cellular adaptation during infection
456 [62]. We hypothesize this collection of three hallmarks may serve as a guide to identify
457 other pivotal host defense factors. Collectively, we interpret this rare combination of
458 signatures that are associated with OAS1 and now MLKL as strong evidence that
459 necroptosis is an indispensable, not auxiliary, host response that has shaped infection
460 outcomes over millions of years.

461 # Methods

462 ## Protein modeling

463 Published crystal structures of m(ouse) RIPK3 (PDB: 4M66), mMLKL (PBD:4M68) and
464 co-crystal structure for mRIPK3:mMLKL (PDB: 4M69) were used for modeling following
465 pairwise alignment with h(uman)MLKL (PDB: 4BTF) or the predicted structure of hRIPK3
466 [20, 49]. Swiss-Model was used to predict the structure of hRIPK3 and myxoma
467 v(iral)MLKL [64]. UCSF Chimera (https://www.cgl.ucsf.edu/chimera/) was used to perform
468 analysis and visualize structures including rapidly evolving sites [65].

469 ## Positive selection analysis

470 Nucleotide sequences were obtained from NCBI and Ensembl databases (S1 File).
471 Multiple sequence alignments (MSA) were performed using MAFFT iterative refinement
472 method FFT-NS-i and visualized using Geneious Prime 2020.1.2
473 (https://www.geneious.com/) [66]. Indels were removed through manual trimming. dN/dS
474 lineage estimates were obtained using sample primate gene MSA and phylogenetic tree
475 [created using previously described primate lineage relationships [67]]. These served as
476 input for FreeRatio analysis implemented in PAML [42]. Nucleotide substitution (NS) site
477 analysis was performed with PAML using both F3x4 and F61 codon frequency models.
478 MEME and FUBAR analysis were performed using Datamonkey
479 (https://www.datamonkey.org/) to predict positively selected amino acid sites [46, 47, 68].
480 The S1 File contains additional findings from this analysis.

481 ## Identification of poxvirus vMLKL

482 Virologs to human MLKL were identified using tBLASTn and/or BLASTp [69]. Sequences
483 were selected based on returned BLAST parameters (total score, E value and percent

484 identity) and the phylogenetic clustering of the sequences using PhyML [59]. Scaled
485 individual hit visualization was constructed using CoGeBlast [70].

486 **Relative depth analysis**

487 Eptesipox raw sequencing reads, published in Tu *et al.,* were obtained directly from Dr.
488 Chris Upton (University of Victoria, Victoria BC, Canada) and Dr. Yoshinori Nakazawa
489 (CDC, Atlanta, Georgia) [71] . NC_035460.1 was used as the eptesipoxvirus reference
490 sequence to map the reads. Myxoma virus raw sequencing reads were obtained from
491 European Nucleotide Archive (https://www.ebi.ac.uk/ena/browser/home), from Project
492 PRJNA513218 [53]. Accession IDs used for this analysis are SRR8402032,
493 SRR8402033, SRR8402034, and SRR8402035. As a control, AF170726.2 was used as
494 the myxoma virus reference sequence to map the reads. Raw sequencing reads were
495 processed using Trimmomatic-0.39 [72] to remove adaptors. Tanoti short read aligner
496 (https://bioinformatics.cvr.ac.uk/software/tanoti/) was then used to map reads to the
497 reference genome. SAMtools [73] was used to convert between file formats, merge files
498 and calculate coverage per basepair. Bins of 500 nucleotides were created for relative
499 depth analysis, which was calculated by dividing the bins by the mean of the non-ITR
500 genomic region. Data was visualized using gplots [74].

501 **Phylogenetic analysis**

502 Multiple Sequence Alignments were performed using MAFFT, with iterative refinement
503 method L-INS-i, on amino acid sequences retrieved from NCBI and Ensembl databases
504 (S4 File) [66]. Maximum Likelihood trees were inferred by PhyML using 100 bootstrap
505 values [59].

506 **Percent amino acid identity heatmap**

507 Multiple Sequence Alignments were performed using MAFFT, with iterative refinement
508 method L-INS-i, on amino acid sequences retrieved from NCBI database (S2 File) [66].
509 The R package gplots was used to create the heatmap found in Fig 4C [74, 75].

510 **Poxvirus RCD-associated host range gene identification**

511 Host range genes were identified using BLASTp and tBLASTn. Sequences were
512 confirmed using reciprocal BLAST hits. Protein families were found using genomic
513 database annotations and published results for included poxvirus genomes. Domain
514 classification for homologs and protein families were confirmed using NCBI conserved
515 genome database [76]. Results were compared to previous homolog studies performed
516 by Bratke *et al*. 2013 and Haller *et al.* 2014, and can be found in S2 File [54, 55]. Proteins
517 truncated at the N- and C-termini were not included in Fig 4G but can be found in the S2
518 File with appropriate label. An exception is necroptosis inhibitor E3, which is predicted to
519 be N-terminally truncated in *Leporipoxviruses* [55]. Genes residing in the inverted terminal
520 repeats (ITR) are counted as separate genes and thus two instances in order to stay
521 consistent with the Fig 4C initial analysis, where the eptesipoxvirus ITR is included and
522 analyzed. The p28/N1R and Ankyrin-repeat families were annotated using NCBI
523 database annotations. The presence of these domains were confirmed using NCBI
524 conserved genome database or via BLASTp [76]. This analysis includes all proteins
525 possessing a p28/N1R-like or Ankyrin-repeat domain and does not predict if these
526 proteins are functional and/or likely truncated.

527 **High resolution synteny analysis**

528 Reciprocal BLAST hits (RBH) were performed for coding sequences upstream and
529 downstream of vMLKL genomic locations across poxvirus species included in this study.

530 Results can be found in the S2 File. Genomic database annotations and the NCBI
531 conserved genome database were used to confirm results [76]. Gene blocks representing
532 Ankyrin-repeat containing proteins without one distinct hit, but conserved homology
533 across poxvirus species are colored navy.

534 **Whole genome comparison**
535
536 Coregenes 5.0 (https://coregenes.ngrok.io/) was used to compare selected poxvirus
537 genomes [77]. Matches were identified using bidirectional best hit with an e-value = $1x10^5$.
538 RIdeogram [58] was used to visualize the output obtained from Coregenes 5.0.

539 **Cell lines**

540 HT29 and HeLa cell lines were obtained from ATCC. Both cell lines were cultured in
541 Corning DMEM with L-Glutamine, 4.5 g/L Glucose, and Sodium Pyruvate supplemented
542 with 10% FBS and 1X Gibco Antibiotic-Antimycotic solution. Cell lines were maintained
543 at 37°C in a humidified incubator at 5% CO_2.

544 **Cell culture treatments**

545 Cells were treated with either human IFNα [1000 U/mL (PBL Assay Science, USA) or
546 human IFNγ [1000 U/mL (ThermoFisher, USA)] diluted in DMEM and incubated for 24
547 hours. After 24 hours, cell lysates were harvested for western blots as described below.

548 **Western blot analysis**

549 Cells were collected using RIPA Lysis and Extraction Buffer (ThermoFisher, 89901)
550 supplemented with Protease and Phosphatase Inhibitor Cocktail (Abcam, ab201119).
551 Protein concentrations were measured using a Bradford assay. For all blots, 5 μg of
552 protein lysates were loaded onto an SDS-PAGE gel and wet-transferred to 0.45 μM
553 Immobilon-P PVDF membrane (Millipore, IPVH00010) at 200 mA for 90 minutes.

554 Membranes were blocked with blocking buffer (5% milk in TBST) for 30 minutes at RT.
555 Membranes were incubated in primary antibodies at 4°C overnight. The following primary
556 antibodies used: MLKL (GeneTex, GTX107538), STAT1 D1K9Y Rabbit mAb (Cell
557 Signaling Technology, 14994S), P-STAT1 Tyr701 58D6 Rabbit mAb (Cell Signaling
558 Technology, 9167S) and β-Actin (Abcam, ab49900). Membranes were washed three
559 times with TBST for 5 minutes and incubated with Goat Anti-Rabbit IgG (Bio-Rad, 170-
560 6515) for 1 hour at RT. Membranes were washed three times with TBST and incubated
561 with Clarity Max Western ECL Substrate (Bio-Rad, 1705062). Following incubation, blots
562 were imaged using the Chemidoc MP Imager (Bio-Rad).

563 **Acknowledgments**

564 We express gratitude to other members of the Hancks Lab for feedback and discussion
565 through the course of this project. We also thank Dr. Anant Gharpure and Dr. Sherry
566 Haller for their comments on the manuscript. We also thank Dr. Chris Upton and Dr.
567 Yoshinori Nakazawa as well as Dr. Chiara Chiapponi and Dr. Davide Lelli for their
568 assistance with the eptesipoxvirus and hypsugopoxvirus data, respectively.

569 **References**

570
571 1. Danthi P. Viruses and the Diversity of Cell Death. Annu Rev Virol. 2016;3(1):533-
572 53.
573 2. Jorgensen I, Rayamajhi M, Miao EA. Programmed cell death as a defence
574 against infection. Nat Rev Immunol. 2017;17(3):151-64.
575 3. Lamkanfi M, Dixit VM. Manipulation of host cell death pathways during microbial
576 infections. Cell Host Microbe. 2010;8(1):44-54.
577 4. Best SM. Viral subversion of apoptotic enzymes: escape from death row. Annu
578 Rev Microbiol. 2008;62:171-92.
579 5. Barber GN. Host defense, viruses and apoptosis. Cell Death Differ.
580 2001;8(2):113-26.
581 6. Kerr JF, Wyllie AH, Currie AR. Apoptosis: a basic biological phenomenon with
582 wide-ranging implications in tissue kinetics. Br J Cancer. 1972;26(4):239-57.

583 7. Galluzzi L, Vitale I, Aaronson SA, Abrams JM, Adam D, Agostinis P, et al.
584 Molecular mechanisms of cell death: recommendations of the Nomenclature
585 Committee on Cell Death 2018. Cell Death Differ. 2018;25(3):486-541.
586 8. Strasser A, O'Connor L, Dixit VM. Apoptosis signaling. Annu Rev Biochem.
587 2000;69:217-45.
588 9. Pearson JS, Murphy JM. Down the rabbit hole: Is necroptosis truly an innate
589 response to infection? Cell Microbiol. 2017;19(8).
590 10. Nailwal H, Chan FK. Necroptosis in anti-viral inflammation. Cell Death Differ.
591 2019;26(1):4-13.
592 11. Green DR. The Coming Decade of Cell Death Research: Five Riddles. Cell.
593 2019;177(5):1094-107.
594 12. Vanden Berghe T, Linkermann A, Jouan-Lanhouet S, Walczak H, Vandenabeele
595 P. Regulated necrosis: the expanding network of non-apoptotic cell death
596 pathways. Nat Rev Mol Cell Biol. 2014;15(2):135-47.
597 13. Dondelinger Y, Hulpiau P, Saeys Y, Bertrand MJM, Vandenabeele P. An
598 evolutionary perspective on the necroptotic pathway. Trends Cell Biol.
599 2016;26(10):721-32.
600 14. Brault M, Oberst A. Controlled detonation: evolution of necroptosis in pathogen
601 defense. Immunol Cell Biol. 2017;95(2):131-6.
602 15. Green DR, Fitzgerald P. Just So Stories about the Evolution of Apoptosis. Curr
603 Biol. 2016;26(13):R620-R7.
604 16. Koonin EV, Aravind L. Origin and evolution of eukaryotic apoptosis: the bacterial
605 connection. Cell Death Differ. 2002;9(4):394-404.
606 17. Zmasek CM, Godzik A. Evolution of the animal apoptosis network. Cold Spring
607 Harb Perspect Biol. 2013;5(3):a008649.
608 18. Wang H, Sun L, Su L, Rizo J, Liu L, Wang LF, et al. Mixed lineage kinase
609 domain-like protein MLKL causes necrotic membrane disruption upon
610 phosphorylation by RIP3. Mol Cell. 2014;54(1):133-46.
611 19. Sun L, Wang H, Wang Z, He S, Chen S, Liao D, et al. Mixed lineage kinase
612 domain-like protein mediates necrosis signaling downstream of RIP3 kinase.
613 Cell. 2012;148(1-2):213-27.
614 20. Murphy JM, Czabotar PE, Hildebrand JM, Lucet IS, Zhang JG, Alvarez-Diaz S, et
615 al. The pseudokinase MLKL mediates necroptosis via a molecular switch
616 mechanism. Immunity. 2013;39(3):443-53.
617 21. Cai Z, Jitkaew S, Zhao J, Chiang HC, Choksi S, Liu J, et al. Plasma membrane
618 translocation of trimerized MLKL protein is required for TNF-induced necroptosis.
619 Nat Cell Biol. 2014;16(1):55-65.
620 22. Chen X, Li W, Ren J, Huang D, He WT, Song Y, et al. Translocation of mixed
621 lineage kinase domain-like protein to plasma membrane leads to necrotic cell
622 death. Cell Res. 2014;24(1):105-21.
623 23. Oberst A, Dillon CP, Weinlich R, McCormick LL, Fitzgerald P, Pop C, et al.
624 Catalytic activity of the caspase-8-FLIP(L) complex inhibits RIPK3-dependent
625 necrosis. Nature. 2011;471(7338):363-7.
626 24. Kaiser WJ, Upton JW, Long AB, Livingston-Rosanoff D, Daley-Bauer LP, Hakem
627 R, et al. RIP3 mediates the embryonic lethality of caspase-8-deficient mice.
628 Nature. 2011;471(7338):368-72.

629 25. Maelfait J, Liverpool L, Bridgeman A, Ragan KB, Upton JW, Rehwinkel J.
630 Sensing of viral and endogenous RNA by ZBP1/DAI induces necroptosis. EMBO
631 J. 2017;36(17):2529-43.
632 26. Kaiser WJ, Upton JW, Mocarski ES. Receptor-interacting protein homotypic
633 interaction motif-dependent control of NF-kappa B activation via the DNA-
634 dependent activator of IFN regulatory factors. J Immunol. 2008;181(9):6427-34.
635 27. Kaiser WJ, Sridharan H, Huang C, Mandal P, Upton JW, Gough PJ, et al. Toll-
636 like receptor 3-mediated necrosis via TRIF, RIP3, and MLKL. J Biol Chem.
637 2013;288(43):31268-79.
638 28. He S, Liang Y, Shao F, Wang X. Toll-like receptors activate programmed
639 necrosis in macrophages through a receptor-interacting kinase-3-mediated
640 pathway. Proc Natl Acad Sci U S A. 2011;108(50):20054-9.
641 29. Guo H, Omoto S, Harris PA, Finger JN, Bertin J, Gough PJ, et al. Herpes simplex
642 virus suppresses necroptosis in human cells. Cell Host Microbe. 2015;17(2):243-
643 51.
644 30. Pearson JS, Giogha C, Muhlen S, Nachbur U, Pham CL, Zhang Y, et al. EspL is
645 a bacterial cysteine protease effector that cleaves RHIM proteins to block
646 necroptosis and inflammation. Nat Microbiol. 2017;2:16258.
647 31. Petrie EJ, Sandow JJ, Lehmann WIL, Liang LY, Coursier D, Young SN, et al.
648 Viral MLKL Homologs Subvert Necroptotic Cell Death by Sequestering Cellular
649 RIPK3. Cell Rep. 2019;28(13):3309-19 e5.
650 32. Koehler H, Cotsmire S, Langland J, Kibler KV, Kalman D, Upton JW, et al.
651 Inhibition of DAI-dependent necroptosis by the Z-DNA binding domain of the
652 vaccinia virus innate immune evasion protein, E3. Proc Natl Acad Sci U S A.
653 2017;114(43):11506-11.
654 33. Upton JW, Kaiser WJ, Mocarski ES. Cytomegalovirus M45 cell death
655 suppression requires receptor-interacting protein (RIP) homotypic interaction
656 motif (RHIM)-dependent interaction with RIP1. J Biol Chem.
657 2008;283(25):16966-70.
658 34. Mack C, Sickmann A, Lembo D, Brune W. Inhibition of proinflammatory and
659 innate immune signaling pathways by a cytomegalovirus RIP1-interacting
660 protein. Proc Natl Acad Sci U S A. 2008;105(8):3094-9.
661 35. Liu Z, Nailwal H, Rector J, Rahman MM, Sam R, McFadden G, et al. A class of
662 viral inducer of degradation of the necroptosis adaptor RIPK3 regulates virus-
663 induced inflammation. Immunity. 2021.
664 36. Fletcher-Etherington A, Nobre L, Nightingale K, Antrobus R, Nichols J, Davison
665 AJ, et al. Human cytomegalovirus protein pUL36: A dual cell death pathway
666 inhibitor. Proc Natl Acad Sci U S A. 2020;117(31):18771-9.
667 37. Elde NC, Child SJ, Geballe AP, Malik HS. Protein kinase R reveals an
668 evolutionary model for defeating viral mimicry. Nature. 2009;457(7228):485-9.
669 38. Hancks DC, Hartley MK, Hagan C, Clark NL, Elde NC. Overlapping Patterns of
670 Rapid Evolution in the Nucleic Acid Sensors cGAS and OAS1 Suggest a
671 Common Mechanism of Pathogen Antagonism and Escape. PLoS Genet.
672 2015;11(5):e1005203.
673 39. Mozzi A, Pontremoli C, Forni D, Clerici M, Pozzoli U, Bresolin N, et al. OASes
674 and STING: adaptive evolution in concert. Genome Biol Evol. 2015;7(4):1016-32.

675 40. Mitchell PS, Emerman M, Malik HS. An evolutionary perspective on the broad
676 antiviral specificity of MxA. Curr Opin Microbiol. 2013;16(4):493-9.
677 41. Sawyer SL, Wu LI, Emerman M, Malik HS. Positive selection of primate
678 TRIM5alpha identifies a critical species-specific retroviral restriction domain. Proc
679 Natl Acad Sci U S A. 2005;102(8):2832-7.
680 42. Yang Z. PAML 4: phylogenetic analysis by maximum likelihood. Mol Biol Evol.
681 2007;24(8):1586-91.
682 43. Knuth AK, Rosler S, Schenk B, Kowald L, van Wijk SJL, Fulda S. Interferons
683 Transcriptionally Up-Regulate MLKL Expression in Cancer Cells. Neoplasia.
684 2019;21(1):74-81.
685 44. Sarhan J, Liu BC, Muendlein HI, Weindel CG, Smirnova I, Tang AY, et al.
686 Constitutive interferon signaling maintains critical threshold of MLKL expression
687 to license necroptosis. Cell Death Differ. 2019;26(2):332-47.
688 45. Rusinova I, Forster S, Yu S, Kannan A, Masse M, Cumming H, et al. Interferome
689 v2.0: an updated database of annotated interferon-regulated genes. Nucleic
690 Acids Res. 2013;41(Database issue):D1040-6.
691 46. Murrell B, Wertheim JO, Moola S, Weighill T, Scheffler K, Kosakovsky Pond SL.
692 Detecting individual sites subject to episodic diversifying selection. PLoS Genet.
693 2012;8(7):e1002764.
694 47. Murrell B, Moola S, Mabona A, Weighill T, Sheward D, Kosakovsky Pond SL, et
695 al. FUBAR: a fast, unconstrained bayesian approximation for inferring selection.
696 Mol Biol Evol. 2013;30(5):1196-205.
697 48. Daugherty MD, Malik HS. Rules of engagement: molecular insights from host-
698 virus arms races. Annu Rev Genet. 2012;46:677-700.
699 49. Xie T, Peng W, Yan C, Wu J, Gong X, Shi Y. Structural insights into RIP3-
700 mediated necroptotic signaling. Cell Rep. 2013;5(1):70-8.
701 50. Murphy JM, Lucet IS, Hildebrand JM, Tanzer MC, Young SN, Sharma P, et al.
702 Insights into the evolution of divergent nucleotide-binding mechanisms among
703 pseudokinases revealed by crystal structures of human and mouse MLKL.
704 Biochem J. 2014;457(3):369-77.
705 51. UniProt C. UniProt: a worldwide hub of protein knowledge. Nucleic Acids Res.
706 2019;47(D1):D506-D15.
707 52. Davies KA, Fitzgibbon C, Young SN, Garnish SE, Yeung W, Coursier D, et al.
708 Distinct pseudokinase domain conformations underlie divergent activation
709 mechanisms among vertebrate MLKL orthologues. Nat Commun.
710 2020;11(1):3060.
711 53. Kerr PJ, Eden JS, Di Giallonardo F, Peacock D, Liu J, Strive T, et al. Punctuated
712 Evolution of Myxoma Virus: Rapid and Disjunct Evolution of a Recent Viral
713 Lineage in Australia. J Virol. 2019;93(8).
714 54. Haller SL, Peng C, McFadden G, Rothenburg S. Poxviruses and the evolution of
715 host range and virulence. Infect Genet Evol. 2014;21:15-40.
716 55. Bratke KA, McLysaght A, Rothenburg S. A survey of host range genes in
717 poxvirus genomes. Infect Genet Evol. 2013;14:406-25.
718 56. Nichols DB, De Martini W, Cottrell J. Poxviruses Utilize Multiple Strategies to
719 Inhibit Apoptosis. Viruses. 2017;9(8).

720 57. Taylor JM, Barry M. Near death experiences: poxvirus regulation of apoptotic
721 death. Virology. 2006;344(1):139-50.
722 58. Zhaodong Hao DL, Ying Ge, Jisen Shi, Dolf Weijers, Guangchuang Yu, Jinhui
723 Chen. RIdeogram: drawing SVG graphics to visualize and map genome-wide
724 data on the idiograms. PeerJ Computer Science. 2020;6:e251.
725 59. Lefort V, Longueville JE, Gascuel O. SMS: Smart Model Selection in PhyML. Mol
726 Biol Evol. 2017;34(9):2422-4.
727 60. Patel MR, Loo YM, Horner SM, Gale M, Jr., Malik HS. Convergent evolution of
728 escape from hepaciviral antagonism in primates. PLoS Biol.
729 2012;10(3):e1001282.
730 61. Darby AC, McInnes CJ, Kjaer KH, Wood AR, Hughes M, Martensen PM, et al.
731 Novel host-related virulence factors are encoded by squirrelpox virus, the main
732 causative agent of epidemic disease in red squirrels in the UK. PLoS One.
733 2014;9(7):e96439.
734 62. Sorouri M, Chang T, Jesudhasan P, Pinkham C, Elde NC, Hancks DC.
735 Signatures of host-pathogen evolutionary conflict reveal MISTR-A conserved
736 MItochondrial STress Response network. PLoS Biol. 2020;18(12):e3001045.
737 63. Chakrabarti A, Jha BK, Silverman RH. New insights into the role of RNase L in
738 innate immunity. J Interferon Cytokine Res. 2011;31(1):49-57.
739 64. Waterhouse A, Bertoni M, Bienert S, Studer G, Tauriello G, Gumienny R, et al.
740 SWISS-MODEL: homology modelling of protein structures and complexes.
741 Nucleic Acids Res. 2018;46(W1):W296-W303.
742 65. Pettersen EF, Goddard TD, Huang CC, Couch GS, Greenblatt DM, Meng EC, et
743 al. UCSF Chimera--a visualization system for exploratory research and analysis.
744 J Comput Chem. 2004;25(13):1605-12.
745 66. Katoh K, Rozewicki J, Yamada KD. MAFFT online service: multiple sequence
746 alignment, interactive sequence choice and visualization. Brief Bioinform.
747 2019;20(4):1160-6.
748 67. Perelman P, Johnson WE, Roos C, Seuanez HN, Horvath JE, Moreira MA, et al.
749 A molecular phylogeny of living primates. PLoS Genet. 2011;7(3):e1001342.
750 68. Weaver S, Shank SD, Spielman SJ, Li M, Muse SV, Kosakovsky Pond SL.
751 Datamonkey 2.0: A Modern Web Application for Characterizing Selective and
752 Other Evolutionary Processes. Mol Biol Evol. 2018;35(3):773-7.
753 69. Altschul SF, Gish W, Miller W, Myers EW, Lipman DJ. Basic local alignment
754 search tool. J Mol Biol. 1990;215(3):403-10.
755 70. Lyons E, Pedersen B, Kane J, Alam M, Ming R, Tang H, et al. Finding and
756 comparing syntenic regions among Arabidopsis and the outgroups papaya,
757 poplar, and grape: CoGe with rosids. Plant Physiol. 2008;148(4):1772-81.
758 71. Tu SL, Nakazawa Y, Gao J, Wilkins K, Gallardo-Romero N, Li Y, et al.
759 Characterization of Eptesipoxvirus, a novel poxvirus from a microchiropteran bat.
760 Virus Genes. 2017;53(6):856-67.
761 72. Bolger AM, Lohse M, Usadel B. Trimmomatic: a flexible trimmer for Illumina
762 sequence data. Bioinformatics. 2014;30(15):2114-20.
763 73. Li H, Handsaker B, Wysoker A, Fennell T, Ruan J, Homer N, et al. The
764 Sequence Alignment/Map format and SAMtools. Bioinformatics.
765 2009;25(16):2078-9.

74. Gregory R. Warnes BB, Lodewijk Bonebakker, Robert Gentleman, Wolfgang Huber, Andy Liaw, Thomas Lumley, Martin Maechler, Arni Magnusson, Steffen Moeller, Marc Schwartz and Bill Venables. gplots: Various R Programming Tools for Plotting Data. R package version 3.0.3 ed2020.
75. Team RC. R: A language and environment for statistical computing. R Foundation for Statistical Computing. Vienna, Austria2013.
76. Lu S, Wang J, Chitsaz F, Derbyshire MK, Geer RC, Gonzales NR, et al. CDD/SPARCLE: the conserved domain database in 2020. Nucleic Acids Res. 2020;48(D1):D265-D8.
77. Contreras-Moreira B, Vinuesa P. GET_HOMOLOGUES, a versatile software package for scalable and robust microbial pangenome analysis. Appl Environ Microbiol. 2013;79(24):7696-701.

Figure captions

Fig 1. Cell death pathways, a mechanism of host defense. (A) Apoptosis is a regulated cell death pathway that acts as a key line of host defense against pathogens and is executed by caspases via an extrinsic or intrinsic route [7]. **(B)** Necroptosis can act as an alternative regulated cell death pathway in the event of inhibition of the apoptosis pathway by pathogens [10] such as poxviruses. E3 [32] and vMLKL [31] are recently described poxvirus factors that inhibit necroptotic signaling.

Fig 2. Rapid evolution of the necroptotic axis, RIPK3 and MLKL, across primate lineages. A) Summary of rapid evolution results for M7 x M8 (F3x4) Likelihood ratio test statistics (2δ) for necroptotic factors across a set of twenty-one matching primate species. **B)** MLKL is upregulated by IFNγ treatment in HeLa and HT29 cell lines. **C)** dN/dS values estimated using PAML across twenty-one primate lineages. Branches colored in red display signatures of positive selection (dN/dS > 1, or greater than or equal to 3 nonsynonymous amino acid changes relative to zero synonymous amino acid changes).

Fig 3. Widespread signatures of positive selection across necroptosis protein sequences. A) Rapidly evolving sites represented as triangles and shown for TRIF (orange), DAI (pink), RIPK1 (red), RIPK3 (green) and MLKL (blue). Rapidly evolving

796 amino acid sites predicted using PAML (yellow triangle), FUBAR (blue triangle) and
797 MEME (green triangle). Sites with p-values < 0.05 or posterior probabilities (P) > 0.95 are
798 listed above the protein cartoons and represented as triangles. Sites with p-values < 0.01
799 or posterior probabilities (P) > 0.99 are bolded and have an asterisk. Amino acid
800 alignment position refers to the human reference sequences. **B)** Location of rapidly
801 evolving sites (shown in red) on the h(uman)RIPK3 (green) homology model and the
802 hMLKL (light blue) crystal structure [20]. The homology model was predicted using Swiss-
803 Model [64] and aligned to crystal structures m(ouse)RIPK3 (silver), mMLKL (silver), and
804 mRIPK3:mMLKL (silver) [49]. **C)** Rapid evolution (red) at the mRIPK3 hydrophobic
805 pocket. **D)** Rapid evolution exclusive to the RIPK3 RHIM-domain proximal to the EspL
806 cleavage motif (Q*G**N - highlighted in black). Sequences spanning the EspL cleavage
807 motif from 12 primates for RIPK3 (green), RIPK1 (red), TRIF (orange), and DAI (pink)
808 RHIM domains. The EspL cleavage site is underlined and displays a black arrow above
809 the amino acid. Sites with p-values < 0.05 or posterior probabilities (P) > 0.95 are listed
810 above the protein cartoons and represented as triangles. Sites with p-values < 0.01 or
811 posterior probabilities (P) > 0.99 are bolded and have an asterisk. Amino acid alignment
812 position refers to the human reference sequences. Note: PAML, MEME, and FUBAR
813 analysis were performed for RIPK1 without drill monkey, since this region was trimmed in
814 previous analyses.

815 **Fig 4. vMLKL mimics are encoded in *Avipoxvirus*, Clade II, eptesipoxvirus, and**
816 **hypsugopoxvirus genomes. A)** Protein structures of human MLKL (light blue) and
817 myxoma v(irus)MLKL (dark blue). **B)** Homology model for myxoma vMLKL (dark blue)
818 predicted using Swiss-Model and aligned onto previously published crystal structures for

hMLKL (light blue) and mMLKL (silver). **C)** Heatmap comparing percent identities of vMLKL copies across poxvirus species which were included in this study. **D)** Cladogram depicting distinct species containing a vMLKL copy with *Avipoxvirus* (green), Clade II (blue) and other poxvirus species (yellow, pink and red) separated according to genus. Note that eptesipoxvirus and hypsugopoxvirus contain multiple copies of vMLKL and are labeled based on their position in the chromosome – A (yellow), B (pink), C (red). Eptesipoxvirus (black dashed box) contains vMLKL copies located on the inverted terminal repeats (ITR) represented by A (yellow) and C (red). **E)** Location of individual and multiple copies of vMLKL across poxvirus genomes. Multiple copies of vMLKL are highlighted (yellow, pink, and red) in eptesipoxvirus and hypsugopoxvirus**.** Chromosomal cartoons created in CoGeBlast represent scaled locations of the vMLKL copies for each of the poxvirus species. The genome accession numbers are located on the top left corner of the chromosomes, and the nucleotide lengths are located on the top right corner of the chromosomes. **F)** Multiple copies of vMLKL in the eptesipoxvirus genome are supported by relative depth analysis. The distribution of reads that align with the ITR and non-ITR regions is shown. Zoomed in images, represented by black boxes, show the relative depth of the EPTV vMLKLs (black) and the two flanking upstream and downstream genes (gray). The ITR relative depth mean is 1.852 and the median is 1.899. The non-ITR relative depth mean is 1.000 and the median is 1.025. **G)** Repertoire of poxvirus apoptosis and necroptosis antagonists explained, in part, by evolutionary distribution of vMLKL. Only proteins predicted to be functional are shown. Two exceptions, found in myxoma virus and rabbit fibroma virus, are represented by an '*' and have N-terminally truncated E3 copies. In depth analysis can be found in S2 File.

842 **Fig 5. High resolution synteny analysis suggests diverse evolutionary histories for**
843 **vMLKL**. Analysis of upstream and downstream flanking genes indicate vMLKLs (black)
844 reside at different locations across poxvirus genomes. Protein homology was determined
845 using reciprocal BLAST hits for the 5 genes upstream (left of vMLKL) and 5 genes
846 downstream (right of vMLKL) of vMLKL. While a gene window of 11 is shown here, an
847 expanded analysis is found in the S3 File. Genes oriented to the right represent 5'-3'
848 directionality while genes oriented to the left represent 3'-5' directionality. The letter "U"
849 represents a gene that is either unique to the individual species or unique to the group of
850 poxviruses that have maintained a vMLKL copy. Gene blocks that have homologous
851 genes (colored borders) that are outside the scope of this figure have arrows pointing to
852 the left (representing upstream) or to the right (representing downstream). Two
853 Yatapoxvirus species (Yaba monkey tumor virus and Yaba-like disease virus) were
854 included as they belong to clade II but lack vMLKL. ⚳ represents a deletion event.
855 Species defined as "Other" (red) are either unclassified (hypsugopoxvirus) or part of
856 vespertilionpoxviruses (eptesipoxvirus).

857 **Fig 6. Phylogenetic analysis suggests a singular origin for non-orthologous**
858 **poxvirus MLKLs.** A maximum-likelihood phylogenetic tree of diverse host and poxviral
859 MLKL amino acid sequences produced using PhyML [59] is displayed. Consistent with a
860 single horizontal gene transfer event, *Avipoxvirus* (green), Clade II (blue), and other
861 poxvirus sequences (yellow, pink, and red) cluster together. Branch lengths represent
862 amino acid changes per site. 100 bootstrap replicates were performed with branch
863 support > 70% (*) or 90% indicated (**). The alignment of MLKL sequences was
864 performed using MAFFT and can be found in the S4 File.

865 **Fig 7. Amino acid variant analysis suggests Avipox vMLKL is the original locus,**
866 **and Clade II vMLKL is an independent, but derived copy.** A set of informative amino
867 acid positions were identified in the alignment of mammalian and vMLKL sequences.
868 Residues identical to consensus are shown as "." while "-" represents a gap in the
869 sequence alignment. Amino acid site positions (shown above the alignment) are in
870 relation to human MLKL. Alignment can be found in the S4 File.

871 **Fig 8. Volatile evolution of MLKL and hallmarks associated with key host defense**
872 **factors indicate that necroptosis is a pivotal, not auxiliary, immune defense. A)**
873 Model of poxvirus MLKL acquisition and evolution across lineages. Data indicate that
874 vMLKL was likely acquired by a vertebrate host presumably through a single horizontal
875 gene transfer event to a poxvirus ancestor (Fig.6). This copy at the original site of
876 integration, located on the right arm, has been maintained in *Avipoxvirus* (green)
877 genomes over time to present day (Fig 4). A duplication followed by a deletion event
878 occurred in the common ancestor of Clade II (dark blue) and species classified as "Other"
879 (red) following divergence from *Avipox* (Figs 5 and 7, S5 Fig). This second copy also on
880 the right arm has been maintained until the present in all Clade II species but lost in
881 Yatapoxvirus lineages (Fig.5). Subsequently, the second copy was duplicated to the ITR
882 in the ancestor of eptesipoxvirus and hypsugopoxvirus, which is maintained in present-
883 day lineages. While hypsugopoxvirus ITR sequence was not included in the final genome
884 assembly, our synteny analysis (Fig 5) suggests vMLKL is also located on an ITR (dashed
885 box) in this lineage. "✂" represents predicted deletion events. Dashed arrows represent
886 the progression of evolutionary time (left to right). Scaled chromosomal locations of the
887 present day vMLKL copies are represented on the right. **B)** MLKL displays all three key

888 hallmarks often common to key host defense factors but unique to OAS1 [38, 39, 61],
889 MISTRAV, and MISTR1 [62]. These factors are rapidly evolving, possess a viral
890 homolog/virolog, and are regulated by immune signals (includes upregulation and
891 downregulation).

892 ## Supporting information

893

894 **S1 Fig. MLKL and RIPK3 rapidly evolving sites localize to protein surfaces.**
895 Positively selected sites (red) identified in Fig 3 mapped onto filled crystal structures of
896 RIPK3 and MLKL.

897 **S2 Fig. Protein sequence alignments for human MLKL, mouse MLKL and vMLKLs.**
898 **A)** Diagrams of hMLKL (light blue) and mMLKL (silver) with previously established
899 functional residues annotated [19-21, 49-51]. Amino acid alignment of hMLKL, mMLKL,
900 and poxvirus MLKLs was constructed using MAFFT, with functional residues annotated
901 on diagrams also highlighted on this alignment. Brackets correspond to the starting point
902 of vMLKL, which is truncated, relative to hMLKL (alignment beginning at hMLKL N155).
903 **B)** Alignment of human MLKL F386 (corresponding to mouse MLKL F373) with MLKLs
904 from diverse host species. Aromatic amino acid positions (red) are primarily conserved to
905 Aves.

906 **S3 Fig. Relative depth analysis of myxoma virus genome sequencing reads**
907 **indicates a single copy of vMLKL in this species. A)** Table shows MYXV and EPTV
908 read depth (total number of reads in the BAM file) and effective depth (number of reads
909 in the BAM file that map to the reference genome) following merging of bam files. Analysis
910 performed using data from Kerr *et al.*, and Tu *et al.,* [53, 71]. Myxoma virus analysis was
911 performed as a control given complementary analysis (Fig 4F) and predicted single-copy

912 vMLKL in this and other clade II poxviruses. As the effective depth for myxoma virus
913 sequencing was lower than eptesipoxvirus data, read depth isolates were pooled together
914 to facilitate a more normalized approximation of the read counts per nucleotide in the
915 genome. **B)** Myxoma virus genome relative depth analysis - (reads that align with the ITR
916 and non-ITR regions), where "n =" represents the number of myxoma virus isolates
917 pooled together from Project PRJNA513218 [53]. Inset, relative depth at MYVX vMLKL
918 (black) locus including two flanking upstream and downstream genes (gray). The non-
919 ITR and ITR means and medians are present on each plot.

920 **S4 Fig. Poxvirus Ankyrin and P28/N1R protein family ranges separated by genus.**
921 Summary of ankyrin-repeat containing and P28/N1R proteins per genome analyzed in
922 Fig 4G. Functional protein predictions were not performed for these families.

923 **S5 Fig. Whole genome synteny analysis illustrates the presence of distinct,**
924 **multiple copies of vMLKL across poxvirus genomes.** The whole genome
925 comparisons are **A)** canarypox virus (*Avipoxvirus* - green) versus myxoma virus (Clade II
926 - blue), **B)** yaba-like disease virus (Clade II - blue) versus myxoma virus and **C)**
927 eptesipoxvirus (Other - red) versus myxoma virus. Sequence accession numbers are
928 centered at the bottom of each genome. Lines that extend between genomes represent
929 homologous regions, that were calculated using CoreGenes 5.0
930 (https://coregenes.ngrok.io/) [77]. Lines that are light gray represent conserved
931 homologous regions that are not part of the Fig 5 high resolution synteny analysis. Lines
932 in dark gray represent conserved homologous genes that are shown in Fig 5 and the S3
933 File. vMLKL is represented by a black line. "" represents a deletion event.

934 **S1 File. Supporting analysis for Figs 2 and 3 and S1 Fig.**

935 **S2 File. Supporting analysis for Fig 4 and S4 Fig.**

936 **S3 File. Supporting analysis for Fig 5.**

937 **S4 File. Supporting analysis for Figs 6 and 7.**

Palmer et al. Fig 1

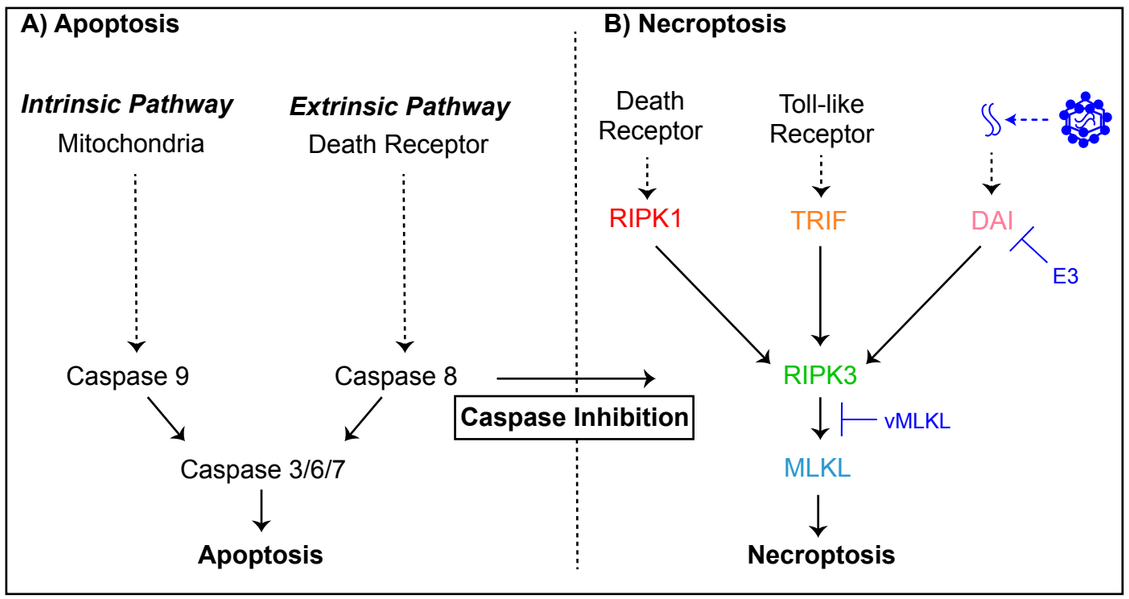

Palmer et al. Fig 2

A)

	2δ	P-value
TRIF	5.481	0.065
DAI	10.311	**5.767×10^{-3}**
RIPK1	5.434	0.066
RIPK3	39.212	**3.056×10^{-9}**
MLKL	42.679	**5.400×10^{-10}**

B)

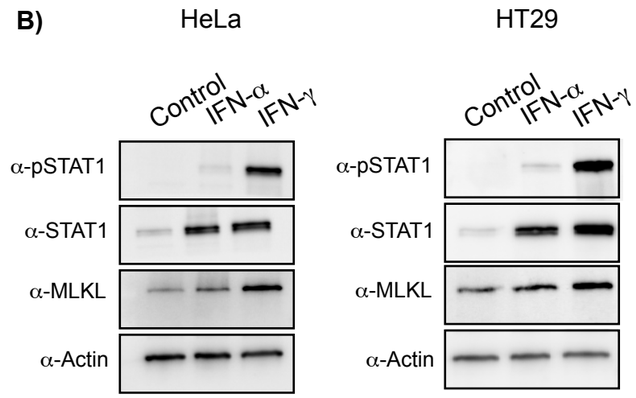

C)

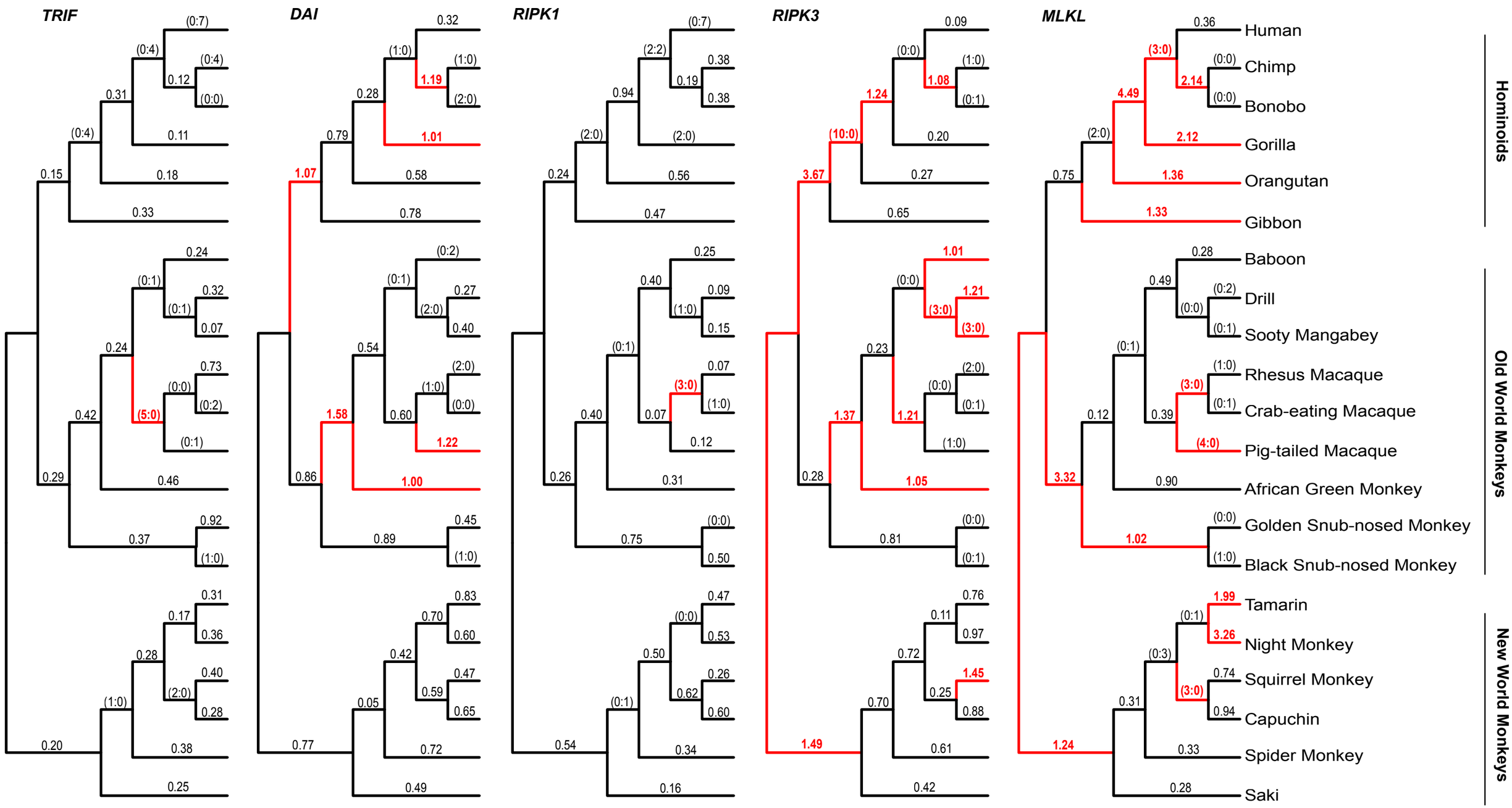

Palmer et al. Fig 3

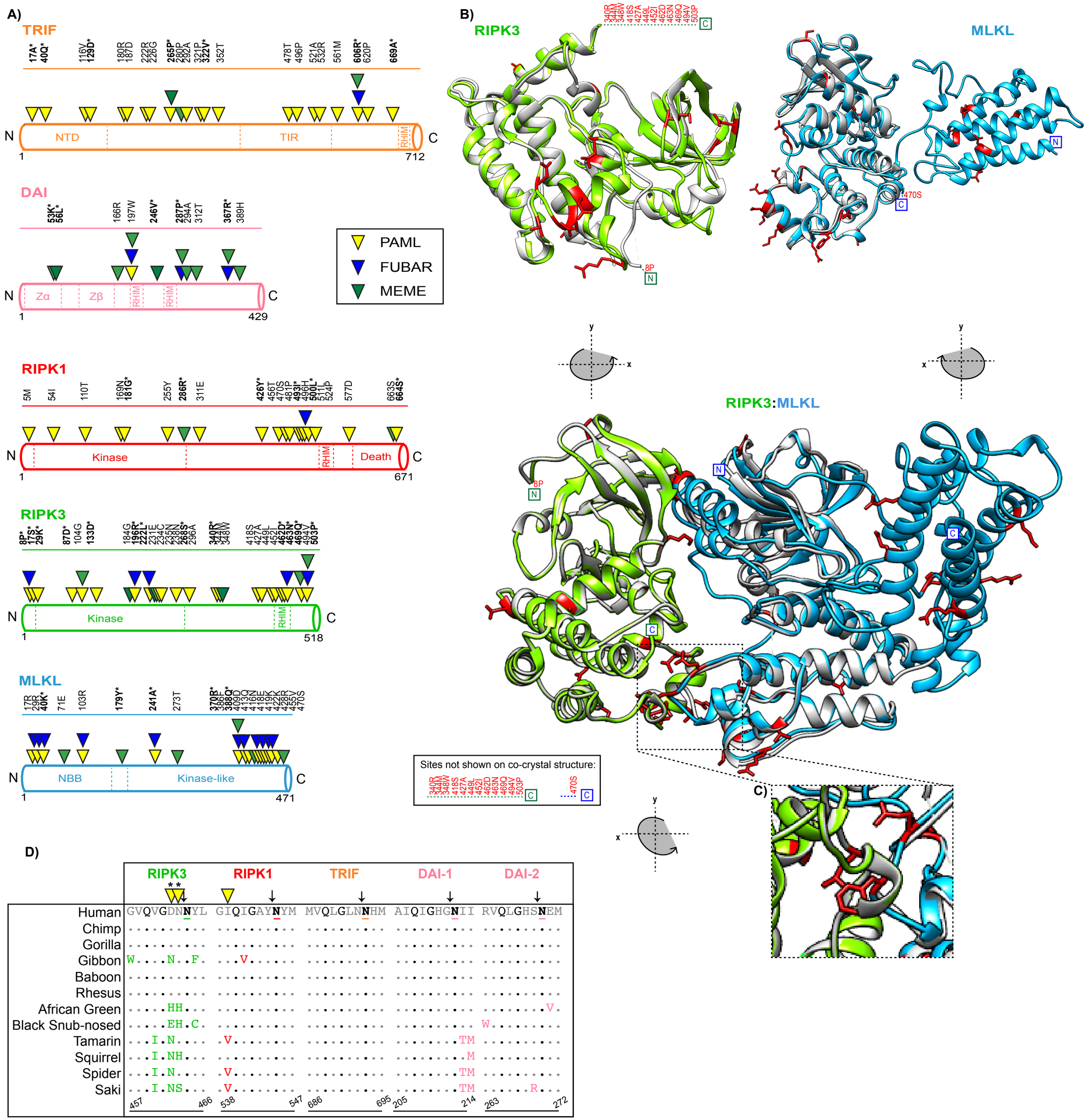

Palmer et al. Fig 4

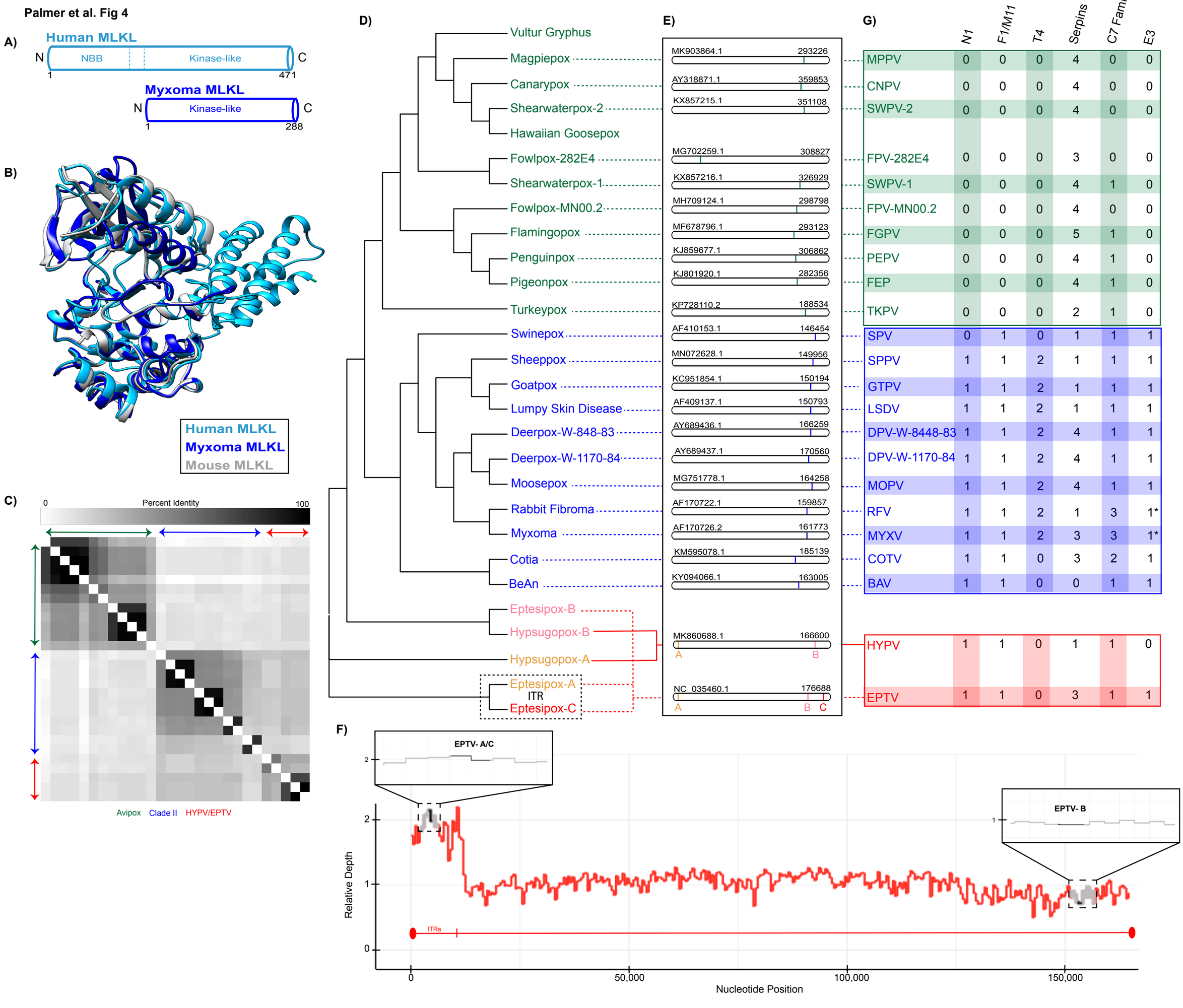

Palmer et al. Fig 5

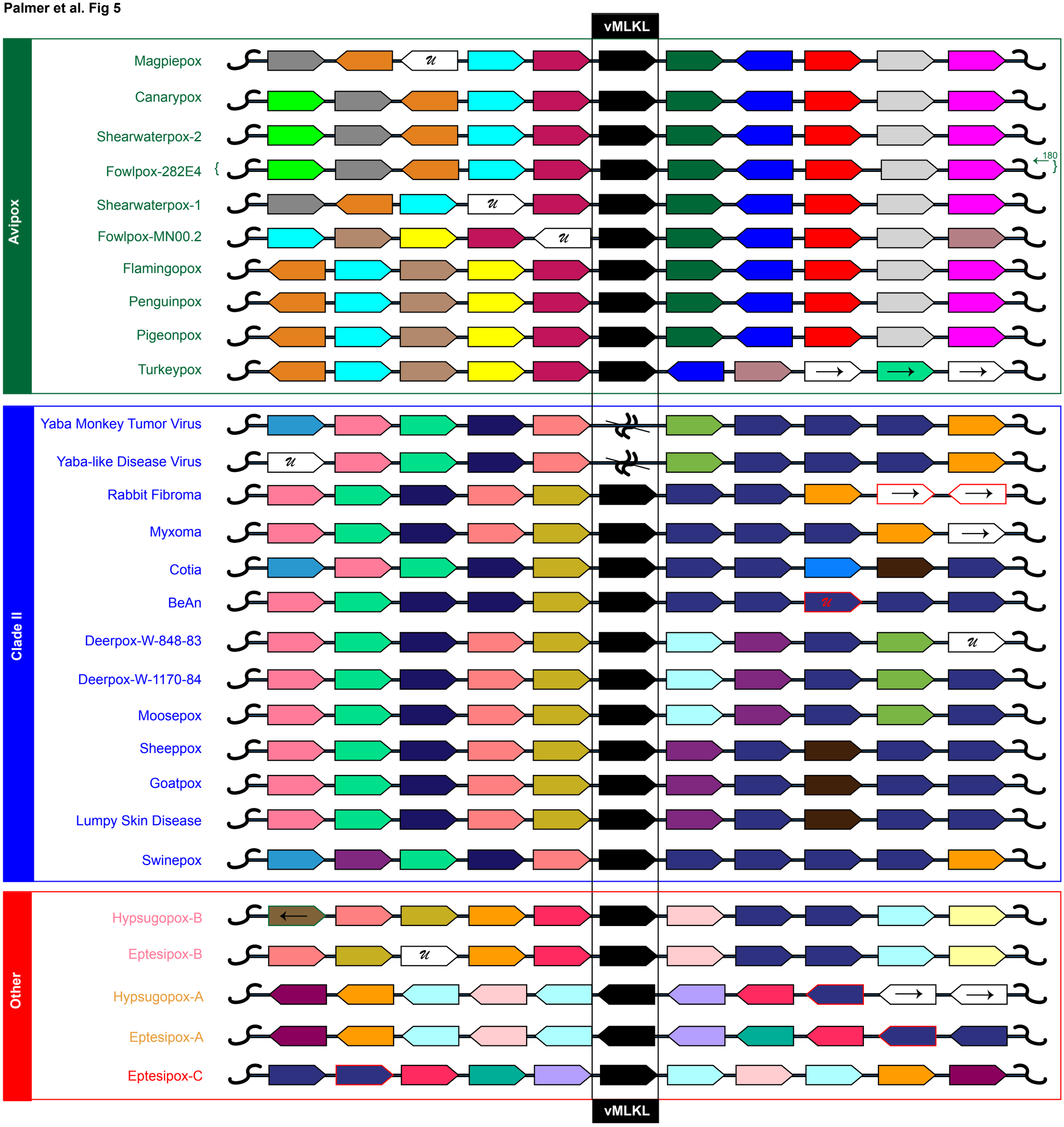

Palmer et al. Fig 6

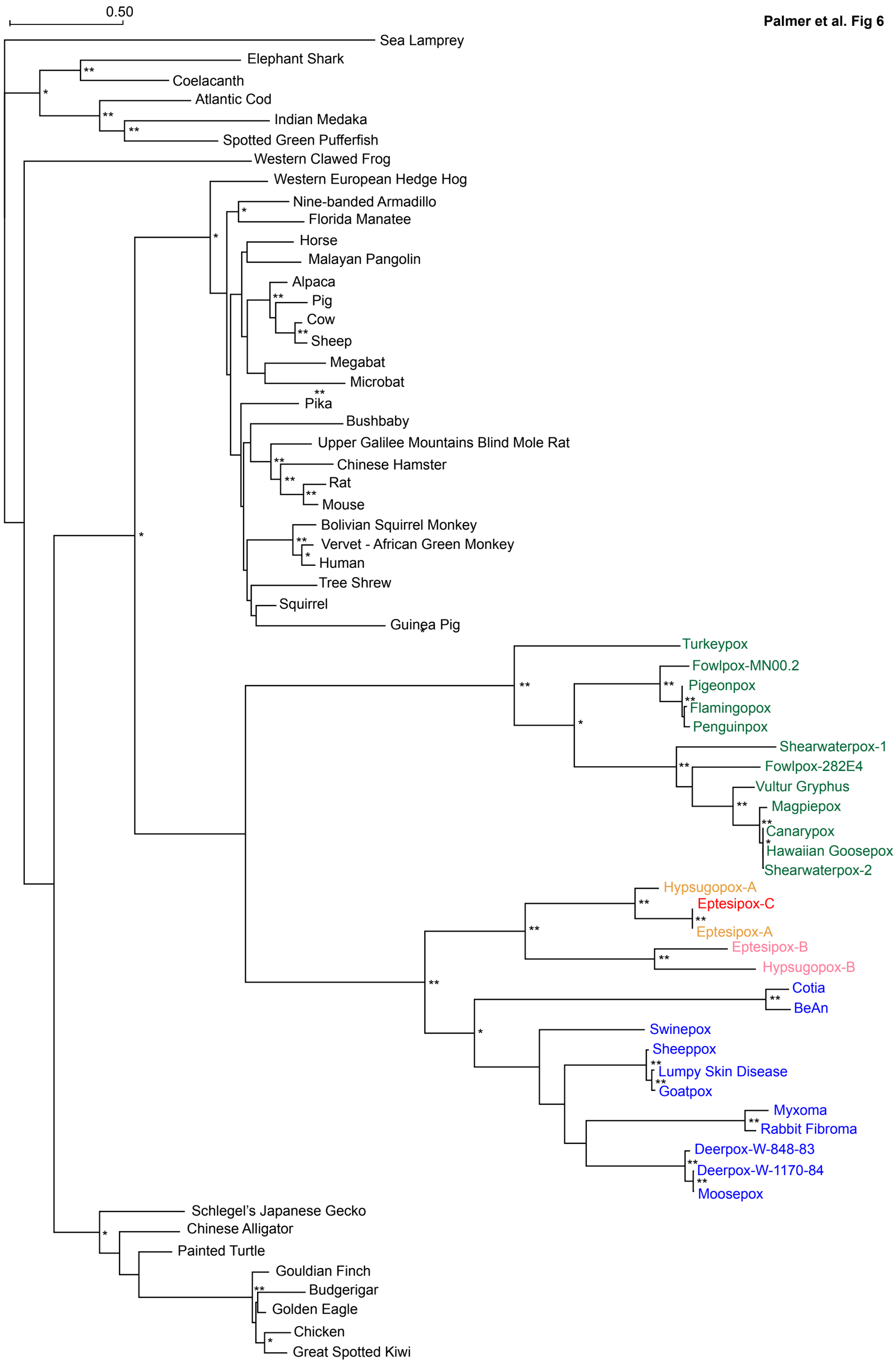

Palmer et al. Fig 7

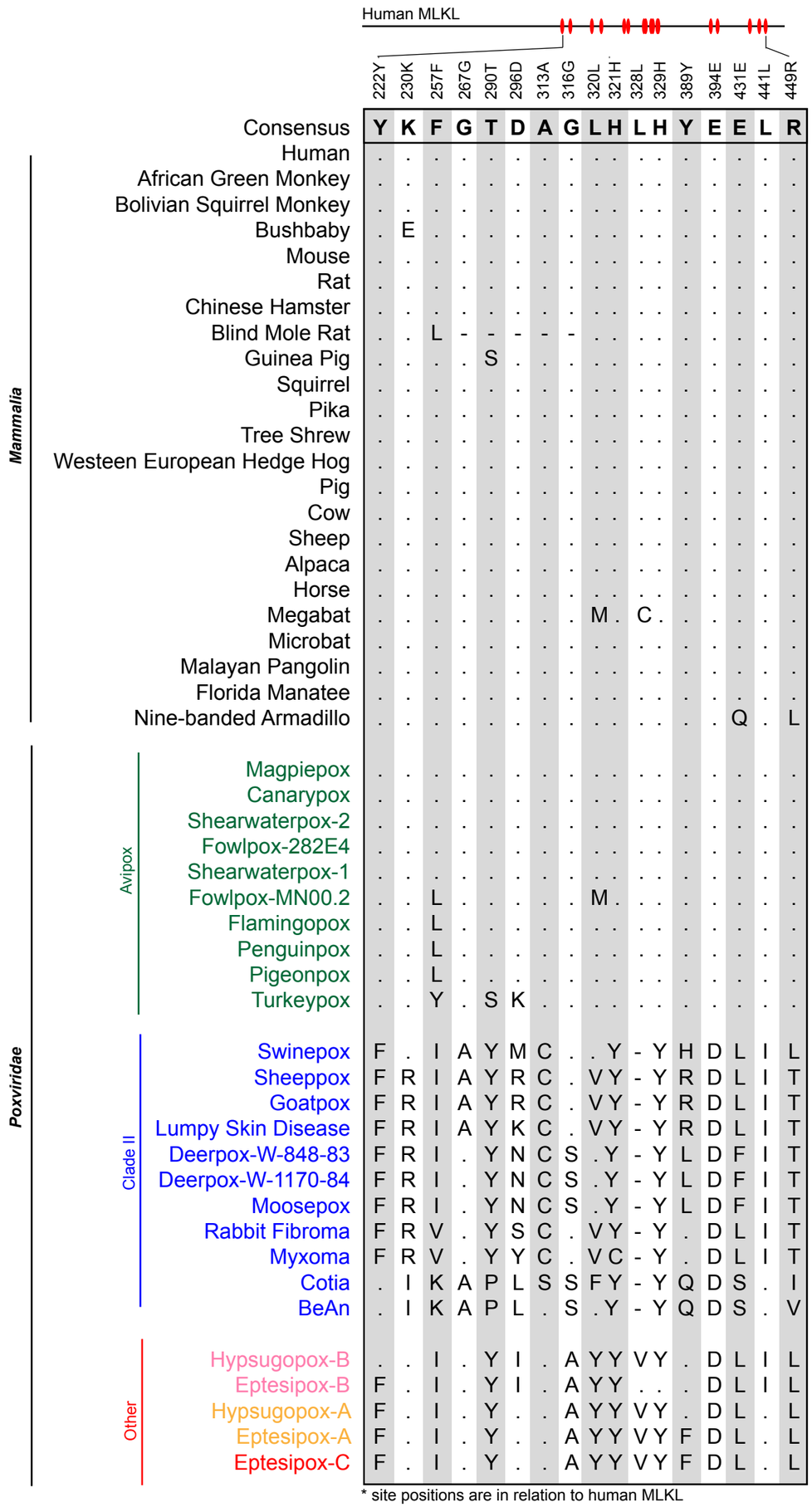

* site positions are in relation to human MLKL

Palmer et al. Fig 8

A)

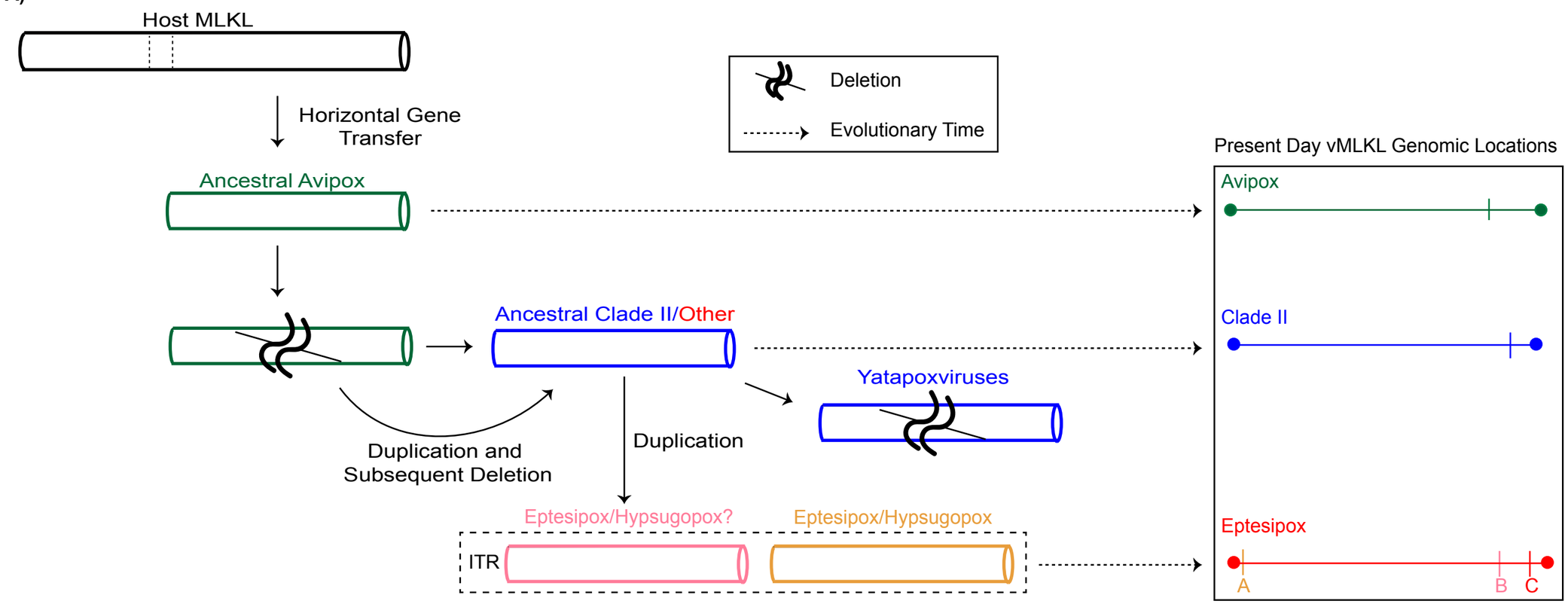

B)

	Rapidly Evolving (dN/dS > 1)	Virologs vMLKL	Regulated by Interferon Signals
APOBEC3G	+	-	+
cGAS	+	-	+
DAI	+	-	+
MAVS	+	-	-
MLKL	+	+	+
MxA	+	-	+
OAS1	+	+	+
PKR	+	-	+
TRIM5α	+	-	+
MISTRAV	+	+	+
MISTR1	+	+	+

Palmer et al. S1 Fig

A)

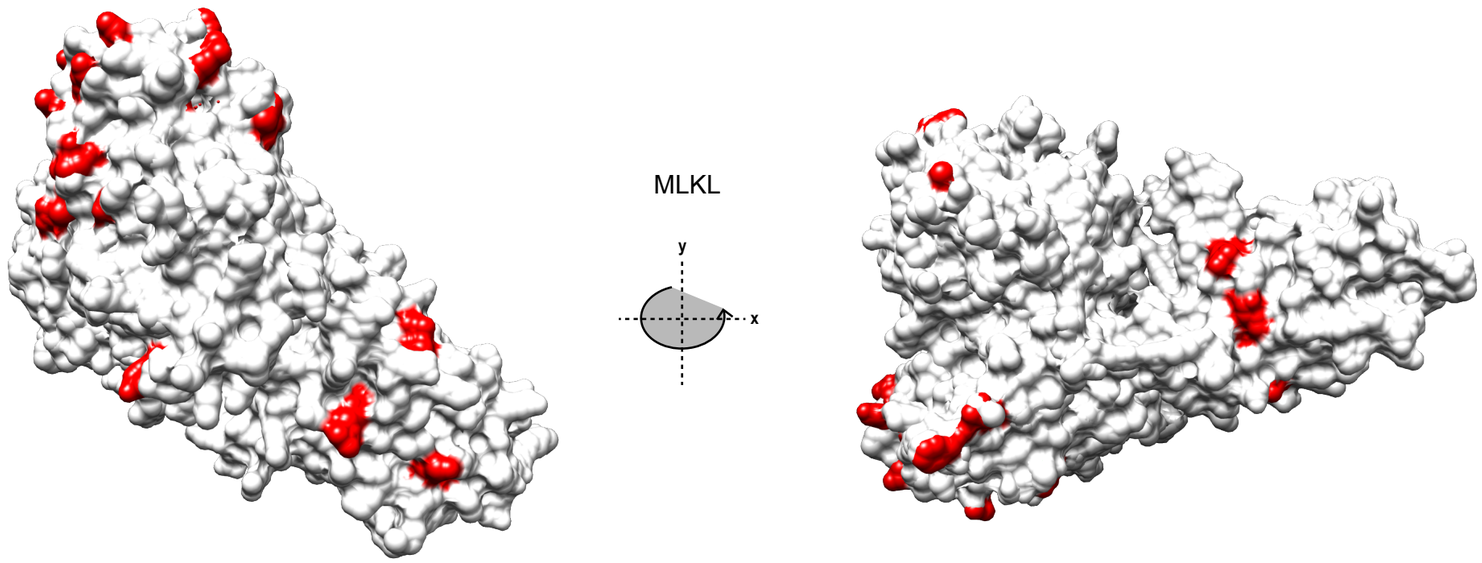

B)

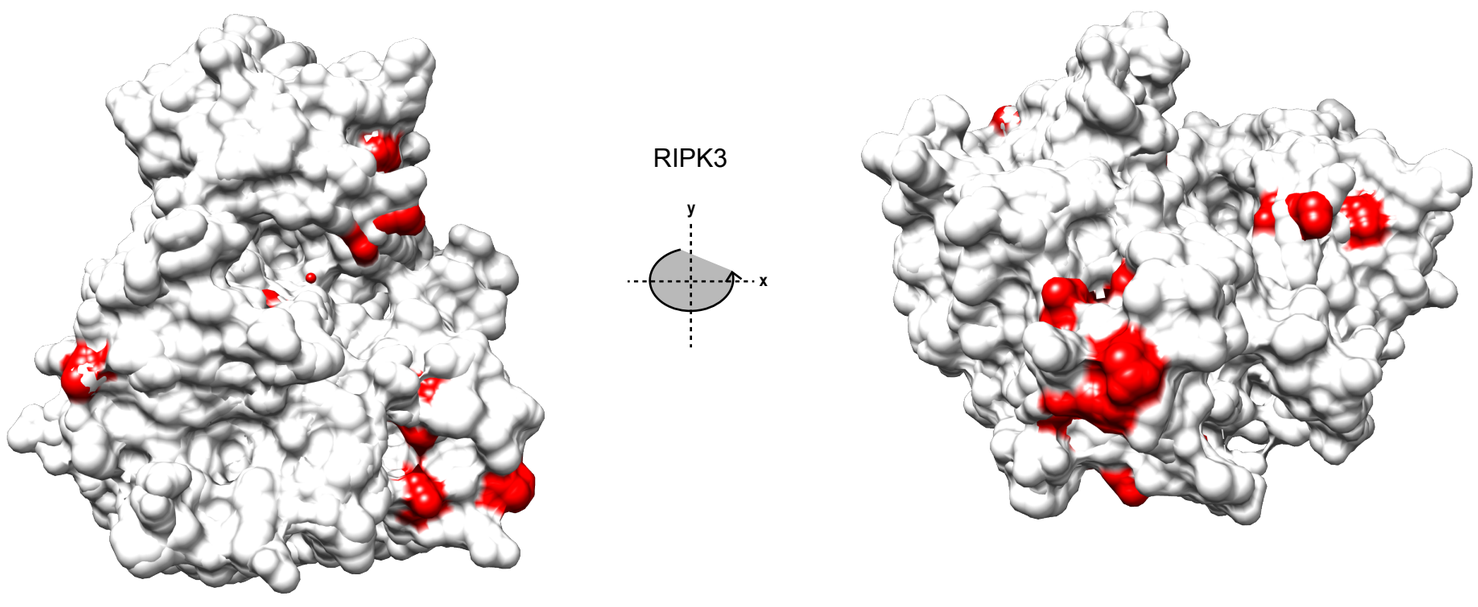

Palmer et al. S2 Fig

A)

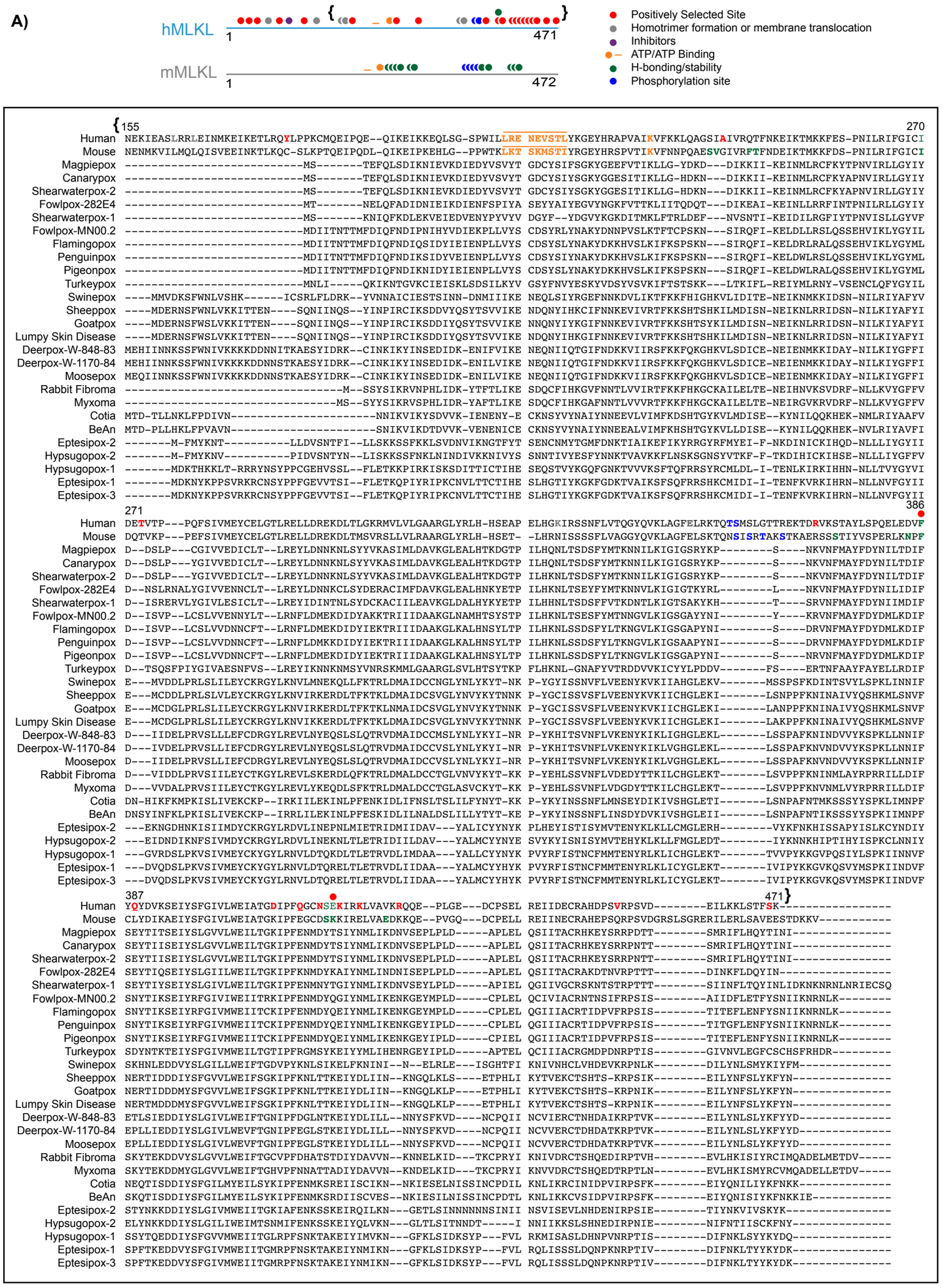

B)

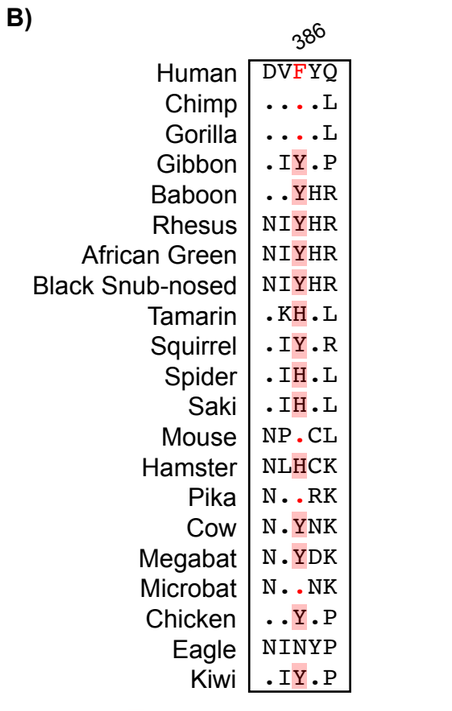

Palmer et al. S3 Fig

A)

Species	Number of Isolates	Read Depth	Effective Depth
Eptesipox	1	15,580,507	952,609
Myxoma	1	827,204	690,356
	2	1,821,118	1,659,533
	3	2,441,318	2,230,935
	4	3,424,938	3,102,827

B)

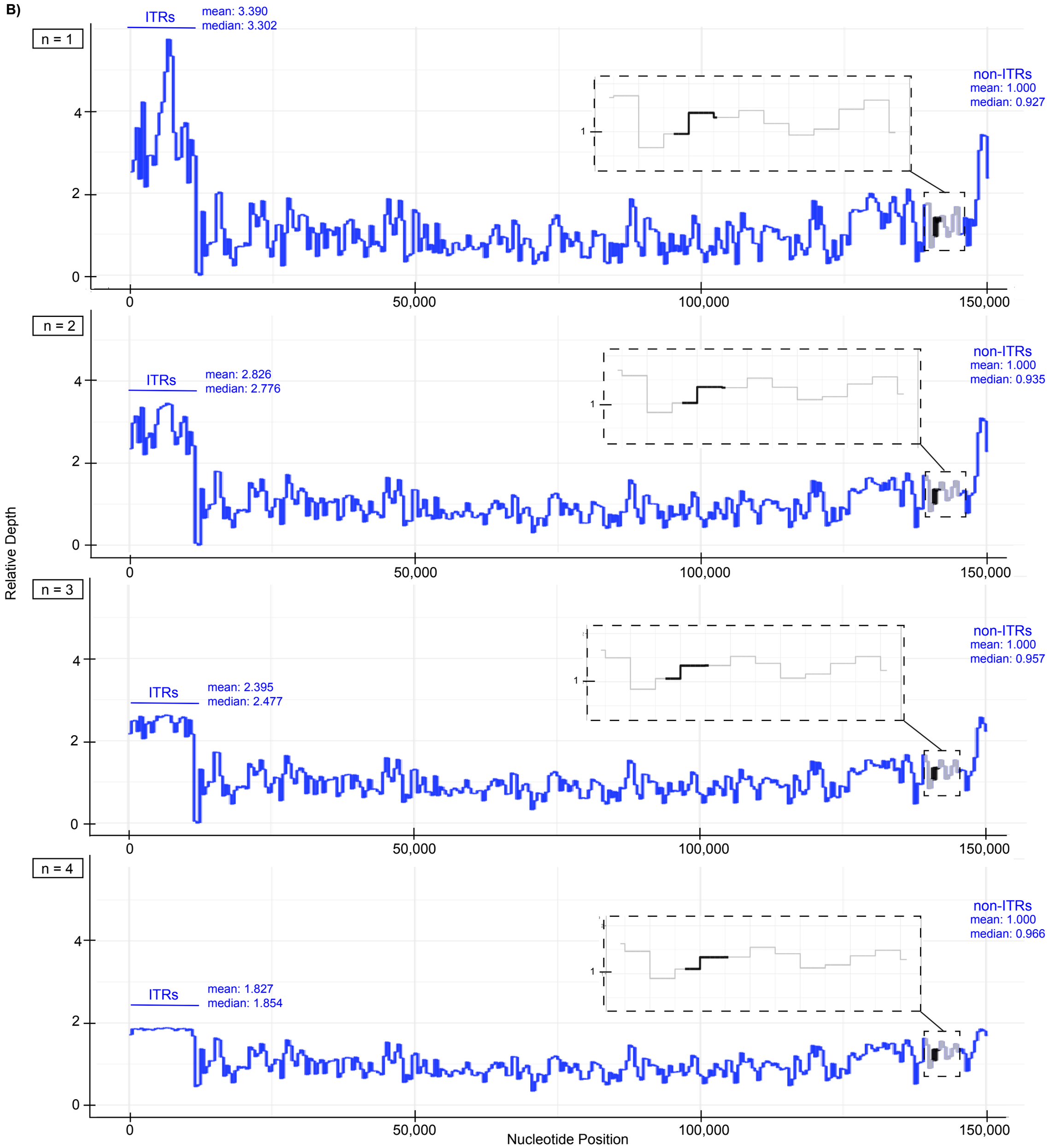

Palmer et al. S4 Fig

	Avipox	Clade II	HYPV/EPTV
Ankyrin Protein Family (proteins/genome)	16-62	4-16	4-8
P28/N1R Family (proteins/genome)	3-26	1-2	1
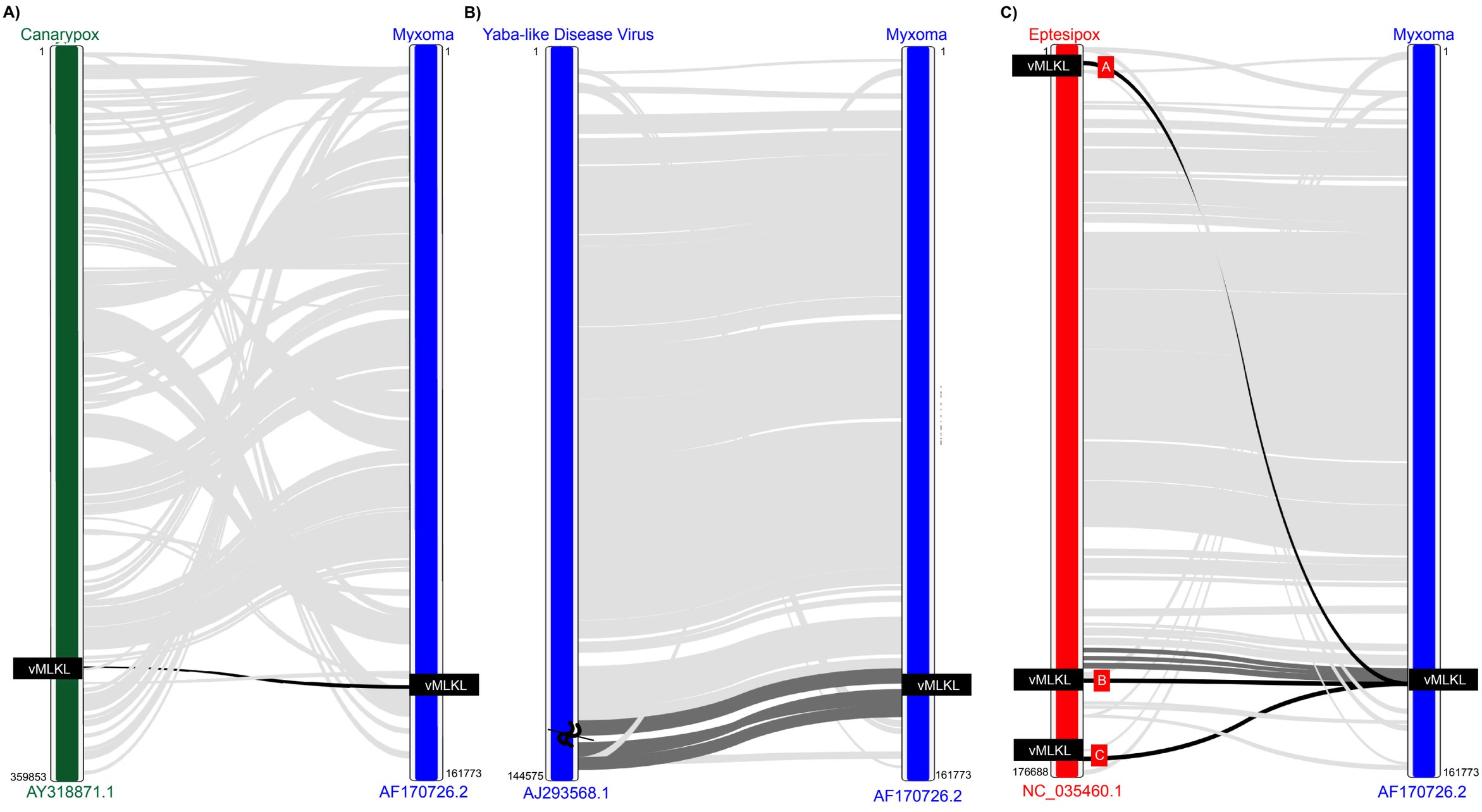
Palmer et al. S5 Fig